Indian Journal of Biochemistry & Biophysics
Vol. 62, November 2025, pp. 1233-1257
DOI: 10.56042/ijbb.v62i11.17496

Heterocyclic organic compounds extracted from *Artemisia judaica* (L.) induced caspase-dependent mitochondrial pathway in different breast and liver cancer cell lines: *In silico* and *in vitro* studies

Fouzi S Aboud[1,2]*, Majed A Al-Shaeri[1,3], Ali T Zari[1,4,5], Ehab MM Ali[6,7] & Naif A Almalki[6,8]

[1]Department of Biological Sciences; [3]Environmental Protection and Sustainability Research Group, Faculty of Science; [4]Centre of Excellence in Bionanoscience; [5]Princess Dr. Najla Bint Saud Al-Saud Centre for Excellence Research in Biotechnology; [6]Department of Biochemistry, Faculty of Science; & [8]Experimental Biochemistry Unit, King Fahd Medical Research Centre, King Abdulaziz University, Jeddah-21589, Saudi Arabia

[2]Department of Anatomy, Histology and Embryology, Faculty of Medicine, University of Tripoli, Tripoli-13932, Libya

[7]Department of Chemistry, Faculty of Science, Tanta University, Tanta-31527, Egypt

Received 27 February 2025; *revised 19 May 2025*

Oestrogen-dependent cancers, such as breast and liver cancer, depend on oestrogen to develop and grow rapidly. This study evaluated the anticancer activity of extracted heterocyclic compounds from *Artemisia judaica* (L.) as alternative drug candidates against different oestrogen-sensitive cancer cells. Fresh *A. judaica* leaves were macerated in 80% ethanol and evaporated using an incubator at 40°C to obtain a yellow brown crude extract. Tri-spectroscopy and molecular analytical techniques were used to identify the extracted compounds' bioactive constituents and binding stability. Different normal HSF, and cancer cell lines MCF-7, T47D, MDA-MB-231, and HePG2 were treated with various concentrations of doxorubicin and *A. judaica* extract for twenty-four h and forty-eight h. The cytotoxic activity of the extracted compounds was evaluated using bio-viability assays. The extracted heterocyclic compounds (benzamide, N-[4-(1H-1,3-benzimidazol-2-yl)-1,2,5-oxadiazol-3-yl] -4-fluoro-, 3-phenyl-6-(4-nitro-phenyl) -4H-(1,2,3) triazole (1,5-d) (1,3,4) oxadiazin-4-one, 2-benzofurancarboxylic acid, 7-methoxy-, (3,4,4-trimethyl-1,2-dioxetan-3-yl) methyl ester, and 2-amino-4,6-diphenyl-pyrimidine) exhibited moderate to well-qualified water solubility, well-binding affinity, and stability with caspase-3, and showed no cytotoxic effects on normal HSF cells with a value of 923.9 ± 5.33 µg/mL and a selectivity index (SI > 2). In contrast, significant inhibition in cell proliferation was observed, particularly in MDA-MB-231 cells with values of 152.7 ± 3.18 µg/mL and 55.18±2.03 µg/mL after 24 and 48 h, respectively, with increased levels of ROS, disruption of MMP that led to increased caspase-3 enzyme, and subsequent induction of cell cycle arrest and apoptosis. We found that atoms such as nitrogen in the extracted heterocyclic compounds made them excellent anticancer medications by targeting DNA and inhibiting oestrogen-sensitive cancer cell progression.

Keywords: Aromatic herb, Caspase-3, Cytotoxicity, Molecular dynamics, Oestrogen-sensitive cancers, Tri-spectroscopy

Various breast cancer subtypes can grow in the liver, and tumour intrinsic subtypes dictate preferential dissemination to the vital organs, and cancer cells expressed $HER2^+$, showing the highest rates of metastasis to the liver[1]. The most useful gene signature for liver metastases comprises the genes frequently seen in HER2-enriched breast cancers. Molecular breast cancer cells with ER^+/ $HER2^+$ hormonal receptors have shown worse overall prognosis than those with ER^+/ $HER2^+$ because they are significantly more likely to metastasize to other organs[2]. The molecular subtype, triple-negative breast cancer (TNBC) is characterized by the absence of oestrogen-receptor alpha (ERα). Still, it can also show oestrogen responsivity when expressed by oestrogen-receptor beta (ER β) and G protein-coupled oestrogen receptor 1 (GPER-1). Subsequently, active oestrogen-related receptors (ERRs) can also activate and modify oestrogen signalling pathways in TNBC[3]. Notably, up to 50% of patients diagnosed with various forms of cancer have liver metastases at the beginning of cancer progression[4]. Oestrogens also act on the liver cells. Previous studies have reported oestrogen-binding proteins in the mitochondria[5] and the hepatocellular carcinoma cell line HePG2[6].

Natural products being studied as possible cytotoxic agents have shown promising results in preclinical research. These products are a significant source of

*Correspondence:
Phone: +966-548340356
E-mail: fmiftah@stu.kau.edu.sa; f.miftah@uot.edu.ly

new therapeutic drugs and have motivated many creative approaches in accelerating cancer clinical research[7]. The aromatic *Artemisia judaica* (L.) comprises annual, perennial, and biennial herb species belonging to the Asteraceae (Compositae) family[8]. Different species of this genus produce various chemicals, including terpenoids, quinines, alkaloids, phenols, and flavonoids[9], that exhibit different biological properties. These include antidepressant, anxiolytic, antitubercular, hepatoprotective, gastroprotective, antihypertensive, antiepileptic, insecticidal, antiemetic, antihyperlipidemic, antiparasitic, and antiviral activities[10].

The apoptosis mechanism, a programmed cell death pathway undertaken by living cells, is characterized by a complicated set of morphological changes, including nuclear condensation, fragmentation, plasma membrane blebbing, and generating apoptotic bodies to sustain the regular turnover of cells and embryonic development[11]. This process is activated by either intracellular or extracellular signal pathways initiated by the mitochondrial apoptotic pathway *via* the activation of the caspase family, including caspase-3[12]. The depolarization of mitochondrial membrane potential is enhanced by the overgeneration of reactive oxygen species, which disrupt the outer mitochondrial membrane and releases cytochrome c, which stimulates the activation of caspase-9. The resulting activation of caspase-3 triggers cell cycle arrest and the process of an apoptosis[13].

Despite the available chemo-radiotherapeutics, hormonal, and immuno-interventions for patients with breast cancer, urgent new directions are needed by developing green drug candidates as an alternative synthetic chemotherapy with low side effects. In this study, we investigated the cytotoxic activity of extracted heterocyclic organic compounds from leaves of *A. judaica* to mitigate against different oestrogen-sensitive cancer cells compared to chemotherapeutic drug candidates (Doxorubicin) through the activation of the caspase-3 dependent mitochondrial pathway.

Materials and Methods

Chemicals and reagents

The materials used in this study include ethanol (Sigma-Aldrich®), Dulbecco's Modified Eagle Medium (DMEM) (Gibco Life Technologies®), Dulbecco's Phosphate Buffered Saline (DPBS) (Sigma Aldrich®), Foetal Bovine Serum (FBS) (Sigma Aldrich®), Dulbecco's Phosphate Buffered Saline (DPBS) (Sigma Aldrich®), Trypsin-EDTA (Sigma Aldrich®), Dimethyl Sulfoxide(DMSO) (Sigma-Aldrich®), Doxorubicin (DOX) (Swiss Parenterals Ltd®), CellROS Green (Invitrogen®), JC-1 stain (Invitrogen®), MTT cell growth assay kit (Sigma Aldrich®), Caspase-3 (Caspase-Glo) Assay Kit (Promega®), Propidium Iodide (PI) (Sigma-Aldrich®), and Apoptosis (Annexin V and PI) Assay Kit (Sigma-Aldrich®).

Equipment and software

The following equipment was used in the experiments: Milli Q water (MILLIPORE SAS®), digital orbital shaker (DAIH-SCIENTIFIC®), precision economy incubator (Thermo-Fisher Scientific®), ultraviolet-visible (UV-Vis) spectrophotometer (Bibby Scientific®), Fourier-transform infrared (FTIR) spectroscopy (Thermo-Fisher Scientific®) gas chromatograph mass spectrometer (GC-MS) (Agilent®), a microplate reader (Agilent®), LABOMED inverted microscope (LABOMED®), digital camera (Leica DFC550®), Thermo Fisher Scientific's Applied Biosystems flow cytometry (Waltham®), Flow cytometry (Acta Biosystems®), Amnis Flowsight (FlowSight®). The software used for molecular dynamics and simulation was Research Collaboratory for Structural Bioinformatics–Protein Data Bank (RCSB-PDB), BIOVIA Discovery Studio 2024, PyMOL 2.5.0, CASTp program, PyRx – Virtual Screening Tools program, PubChem, Swiss-ADMET, Microsoft Excel 2016, and Schrodinger software.

Plant collection and identification

The fresh leaves of *A. judaica* werecollected from Yanbugovernorate in Radwa Mountain, in the western region of Al-Madinah Al-Munawwara, Saudi Arabia. A plant taxonomist at the Department of Biology, KAU, classified and authenticated the sample with sample voucher ArJ18003.

Plant extract preparation

A pure ethanolic crude extract from *A. judaica* leaves was thoroughly washed with Milli Q water (MILLIPORE SAS®) to stick dirt particles, then air-dried at room temperature for twenty-one days. The dried leaves were pulverized using a mechanical grinder until a soft powder was obtained and kept in an airtight container in a dry place. A known weight of dried powdered flowers (25 g) was added to 250 mL of 80% ethanol (Sigma-Aldrich®) and macerated for seventy-two h with a digital orbital shaker (DAIH-SCIENTIFIC®). The extracted solution was filtered

with Whatman No. 1 filter paper, and the filtrate was evaporated in the dark using a precision economy incubator (Thermo-Fisher Scientific®) at 40°C for two h until a dry extract was obtained according to the method by Bennour *et al*.[14] stored at -20°C and used prior to the experiments.

Tri-spectroscopy study

Ultraviolet-visible (UV-VIS) spectrophotometry

UV-VIS spectrophotometry (Bibby Scientific®) was performed to identify the main band patterns. Thesampleextracts were examined through UV-visible light at wavelengths between 200 and 800 nm using the same solvent at a ratio of 1:10[15].

Fourier transform infrared (FTIR) spectroscopy

A small quantity of the extract was placed on a sample holder to identify the main functional groups in the ethanolic extraction of studied medicinal plants. Then, the absorbance and transparent analyses were performed using FTIR spectra scanned from 4,000 to 500 cm^{-1} (Thermo-Fisher Scientific®)[16].

Gas chromatography-mass spectrometry (GC-MS)

The bioactive compounds were identified from *A. judaica* extractusing a capillary column expanding gas chromatography-mass spectrometry (GC-MS) (Agilent®). The sample was injected into the spectrometer, utilizing split mode and a 300°C injection port temperature setting. At 280°C, the flow of helium was 1.61 mL/min. After reaching 50°C for the first minute, the temperature rose roughly 10°C every minute until it reached 300°C. The scan mode was conducted for thirty-two minutes, covering a 40-500 *m/z* range. After that, the molecules were defined with the mass spectral database NIST~98[17].

Computational Studies

Protein preparation

The three-dimensional (3D) structure of caspase-3 (1GFW) was downloaded from the RCSB-PDB (https://www.rcsb.org) in PDB format. After that, the protein was accoutred and defected by removing side chains, water, and hetatm using BIOVIA Discovery Studio and PyMOL 2.5.0 software as shown in (Fig. 1).

Ligand preparation

The chemical structure of four selected compounds from *A. judaica* was downloaded from the PubChem website server: https://www.pubchem.ncbi.nlm.nih.gov/, as shown in (Fig. 2). These structures were then processed and prepared using Auto-Dock Vina and PyRx—virtual screening software to determine the binding affinity.

Generation of receptor grid

A grid was created in Glide with a default Van der Waals radius scaling factor of 1.0 and a charge cutoff of 0.25. The minimized structure was then exposed to the OPLS_2005 force field. The ligand active site was surrounded by a cubic box, fitted to 14 × 14 × 14 for docking the ligands: (i) benzamide, N-[4-(1H-1,3-benzimidazol-2-yl)-1,2,5-oxadiazol-3-yl] -4-fluoro-, (ii) 3-phenyl-6-(4-nitro-phenyl) -4H-(1,2,3) triazolo (1,5-d)

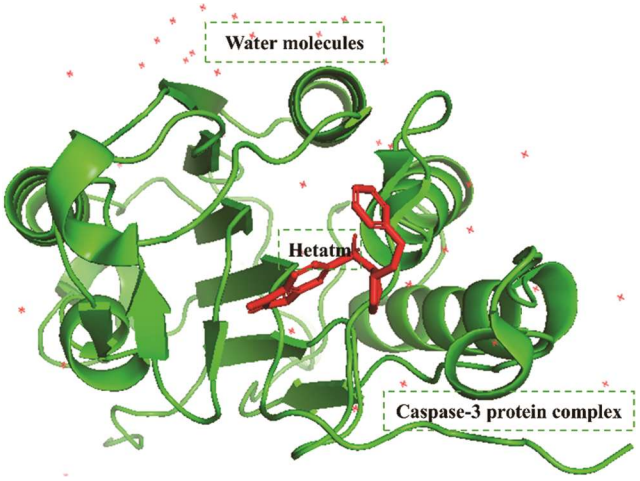

Fig. 1 — Molecular 3D structure of caspase-3 protein from *Homo sapiens*

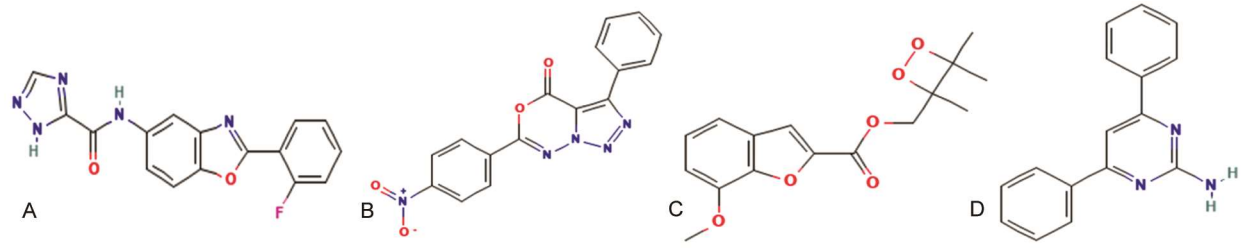

Fig. 2 —Chemical structures of four selected compounds: (A) benzamide, N-[4-(1H-1,3-benzimidazol-2-yl)-1,2,5-oxadiazol-3-yl] -4-fluoro-; (B) 3-phenyl-6-(4-nitro-phenyl) -4H-(1,2,3) triazolo(1,5-d) (1,3,4) oxadiazin-4-one; (C) 2-benzofurancarboxylic acid, 7-methoxy-, (3,4,4-trimethyl-1,2-dioxetan-3-yl methyl ester; and (D) 2-amino-4,6-diphenyl-pyrimidine extracted from *A. judaica* leaves

(1,3,4) oxadiazin-4-one, (iii) 2-benzofurancarboxylic acid, 7-methoxy-, (3,4,4-trimethyl-1,2-dioxetan-3-yl) methyl ester, and (iv) 2-amino-4,6-diphenyl-pyrimidine with 1 GFW protein one by one[18].

Computational pharmacokinetics

The ADMET, which divides pharmaceuticals into categories for absorption, distribution, metabolism, excretion, and toxicity, provides the finest description of the connection between medication dosages and their concentrations over time. First, we consider a chemical's analogues by carefully selecting compounds which can be affected by both *In vitro* and *In vivo* experiment outcomes. Swiss-ADMET is an online server (http://www.swissadme.ch/index.php) that was utilized to evaluate compounds' solubility, bioavailability, and toxicity.

Molecular dynamic simulation

The molecular dynamic (MD) simulations were carried out using Schrodinger software. The orthorhombic box-shaped boundary and the ligand-protein interaction were utilized to resolve the water model. The complex atom buffer box calculation method combined the Na^+ and Cl^- with a 0.15 M salt concentration. At a recorded interval time of 50 ps, the simulation was conducted with an ambient temperature of 300 K and a pressure of 1.01325 bar. The simulation was run using the OPLS-2005 force field[23]. The Root Mean Square Deviation (RMSD) was used to assess the average change in displacement of selected atoms for a particular frame to a reference frame during MD simulations; the Root Mean Square Fluctuation (RMSF) was used to measure the average deviation of a particular residue from its reference position over the trajectory time; secondary structure elements (SSE) was used to monitor the distribution and composition of secondary structure elements; and the ligand torsion profile (LTP) was used to measure the rotation of the ligand around a specific bond.

***In vitro* experiments**

Preparation stock solution

The obtained crude extracts from *A. judaica* were diluted by each 10 mg in 1 mL of Dimethyl Sulfoxide (DMSO) (Sigma-Aldrich®). From stock (20 mg) of doxorubicin (DOX) (SWISS PARENTERALS LTD®), 2.5 µL was added to 2 mL of media to prepare a 50 µg/mL concentration.

Cell culture preparations

The normal human skin fibroblast cell line (HSF), breast cancer (BC) cell lines MCF-7, T47D, MDA-MB-231, and liver cancer (LC) cell line HePG2 were obtained from King Fahd Medical Research Centre (KFMRC); after that, it was kept at 37°C in a water bath until thawing, mixed with 2 mL of Dulbecco's modified Eagle's medium (DMEM) (Gibco Life Technologies®), and then centrifuged for five minutes at 1200 rpm in a 15 mL Falcon tube to fix them. Moreover, a cell culture plate ($T25cm^2$) was used to take a small number of cells from the DMEM, and then trypsin (Sigma Aldrich®) was added to it for anti-proliferative evaluations. The cells were subcultured at three to four-day intervals by washing the monolayers with phosphate-buffered saline (PBS) (Sigma Aldrich®), followed by brief incubation with trypsin. The cells growing at the exponential phase were used to perform all the experiments.

Cell viability assay

The BC cell lines MCF-7, T47D, MDA-MB-231, and the LC cell line HePG2 were seeded with 0.1 mL containing 7,500 cells suspended in complete media, and the plate was then incubated for twenty-four h. Various concentrations ranging from 3,125 to 50 µg/mL of DOX and the pure ethanolic *A. judaica* extracts ranging from 50 to 800 µg/mL dissolved in complete DMEM media were placed in each well containing an attached known number of cells (7,500 cells/well). For each concentration, three wells were repeated with the same concentrations incubated for 24 h. For the normal HSF cell line, the experiment was performed with the same number (7,500 cells) and the same concentrations of DOX and CS extract used for cancer cell lines. The MTT cell viability assay was performed according to Kamiloglu *et al*.[19] by dissolving MTT (5 mg/mL) in Dulbecco's Phosphate Buffered Saline (DPBS, pH 7.4) (Sigma Aldrich®). After that, the MTT solution was filtered through a 0.2 µM filter into a sterile, light-protected container before the testing. At the end of the treatment period (twenty-four and forty-eight h), 10 µL of MTT (3-[4,5-dimethylthiazol-2-yl]-2, 5-diphenyltetrazolium bromide) (Sigma-Aldrich®), was added to each cell well and incubated for three h at 37°C. After that, the formazan product produced by treated cells was dissolved using 100 µL of DMSO by gradually rotating the plates for 10 min. The microplate reader (Bio-RAD®) was used to measure the vitality of the cells at 490 nm. GraphPad Prism 9 was used to calculate the half-maximum inhibitory concentration (IC_{50}) of DOX and *A. judaica* extract. The cell viability was calculated by dividing the

sample absorbance by the control absorbance multiplied by 100, as presented in Equation 1[20].

$$\text{Cell viability} = \frac{\text{Sample absorbance}}{\text{Control absorbance}} \times 100 \quad \ldots (1)$$

Calculation of Selectivity Index

The ratio of sample toxicity concentration to its effective bioactive concentration, which is known as the selectivity index (SI), was determined. The optimal medication should have very low active and relatively high toxic concentrations. In scientific research, SI value should be considered when using medicinal plants or isolated compounds. The SI values were calculated by dividing theIC_{50}value of non-cancerous cells by the IC_{50} value of cancer cells, as presented in Equation 2. Generally, the ratio of IS ranges between 1.96 and 51.3[21].

$$SI = \frac{IC_{50}^{\text{Non-Cancerous cells}}}{IC_{50}^{\text{Cancerous cells}}} \quad \ldots (2)$$

Microscopic examination

After forty-eight h, the morphological changes in cultured HSF, MCF-7, T47D, MDA-MB-231, and HePGE2 cells were examined with a LABOMED inverted microscope (Labomed®) at a magnification of 20x with a scale of 50 µM. The images were captured using a digital camera (Leica DFC550®) at a 12.5-megapixel resolution.

Reactive oxygen species (ROS) assay

To evaluate the intracellular generation of reactive oxygen species (ROS), three small flasks (T25) containing (10^6) MDA-MB-231 cells (of interest) were incubated in a humidified satirized atmosphere for twenty-four h. Each flask was treated with IC_{50} (2 µg/mL) of DOX andIC_{50}(100 µg/mL) of *A. judaica* extract to the culture media and incubated for twenty-four h. After that, 1.5 mL of 0.25% trypsin was added and incubated for five minutes at 37 ºC, then the medium was used to quench the trypsin, and following a five-minute centrifugation at 1500 rpm, the cell suspension underwent two PBS washes. 1 mL of 70% ethanol was added dropwise to each pellet to fix the cells, then stored at -20 °C for one hour. The fixed cells were centrifuged and washed with PBS. Following collection, the treated cell pellet was again suspended in two Eppendorf tubes containing 200 µL of PBS. 200 µL of MDA-MB-231 cell suspension was mixed with 2 µL of 50 mM CellROS Green (Invitrogen®). Stream Flowsite was utilized to assess every experiment on 1×10^4 cells. Three technical and two biological measurements were conducted using Amnis Flowsight (FlowSight®) for the ROS investigation[22].

Mitochondrial membrane potential (MMP) assay

Three small flasks containing (10^6) MDA-MB-231 cells were incubated in a humidified satirized atmosphere for twenty-four h to determine the changes in the mitochondrial membrane. Each flask was treated withIC_{50} (2 µg/mL) of DOX andIC_{50} (100 µg/mL) of *A. judaica* extract to the culture media and incubated for twenty-four h. After that, 1.5 mL of 0.25% trypsin was added and incubated for five minutes at 37°C; then the medium was used to quench the trypsin, and following a five-minute centrifugation at 1,500 rpm, the cell suspension underwent two PBS washes. To fix the cells, 1 mL of 70% ethanol was added dropwise to each pellet. Then, the fixed cells were stored at -20°C for one hour. The fixed cells were centrifuged and washed with PBS. After that, the mixture was incubated at 37°C for thirty minutes, then 200 µL of cell suspension and 2 µL of 20 µM JC-1 stain (Invitrogen®) were combined, and the mixture was incubated at 37°C for thirty minutes to evaluate MMP. Stream Flowsite was utilized to assess every experiment on $1x10^4$ cells. Three technical and two biological measurements were conducted using Amnis Flowsight (FlowSight®)[23].

Caspase-3 activity assay

Caspase activity was measured using the Caspase-Glo Assay Kit (Promega®). The BC cell line MDA-MB-231 (8×10^3) was grown overnight on a ninety-six-well plate and then treated with various concentrations of DOX (1.5 µg/mL, 3 µg/mL, and 6 µg/mL) and *A. judaica* extract (50 µg/mL, 100 µg/mL, and 200 µg/mL) for fourh. CASPASE-GLO 3 reagent was added without removing the medium from the wells and incubated for three h at room temperature. Luminescence was measured using a microplate reader.

Cell cycle assay

Flow cytometry used a DNA binder known as propidium Iodide (PI) (Sigma-Aldrich®) labelling DNA to quantify cell population at cell cycle phases. The BC cell lines MDA-MB-231 ($1 \times 10^{6)}$ were seeded and grown in six-well filtered flasks for twenty-four h, then treated withIC_{50} concentrations of DOX (2 µ g/mL) and *A. judaica* extract (100 µg/mL) for twenty-four h. Following the treatment, the cancer cells were

collected by adding 0.5 mL of 0.25% trypsin and incubated for five minutes; then, complete media was added to stop the action of trypsin. The suspended cells were washed with PBS and centrifuged for five minutes at 1500 rpm. The cells were then fixed at -20°C for one hour in the dark with 1 mL of 70% ethanol, then added to the suspended cells in 100 µL of cold PBS and centrifuged, and then the pellets were suspended with 200 µL of PBS. After that, the cells stained with PI solution (50 µg/mL PI) were added and incubated for fifteen minutes. Flow cytometry (Acta Biosystems®)was used to screen each labelled cell[24].

Detection of apoptosis assay

For detection of the apoptosis, the BC cell line MDA-MB-231(2×10^5) was grown in a six-well plate for twenty-four h and then treated with IC_{50} (2 µg/mL) DOX, IC_{50} (100 µg/mL) *A. judaica* extract, and IC_{50}(100 µg/mL) for twenty-four h. The cells were then harvested using 0.5 mL of trypsin, washed with PBS, centrifuged at 1,500 rpm for five minutes, and suspended in a binding buffer. After gathering the cells in the Falcon tube, the tubes were centrifuged for five minutes at 1,500 rpm. PBS was used to wash the pellets twice. Ultimately, the pellet was suspended into 100 µL of binding buffer and 20 µL of Annexin V and PI (Sigma-Aldrich®) and incubated for twenty minutes. Thermo Fisher Scientific's Applied Biosystems flow cytometry (Waltham®) was used to aspirate the cells. The percentage of viable cells, early and late apoptosis, and necrosis were measured by examining the cells[25].

Statistical analysis

The statistical analysis was done using GraphPad Prism 8 and Microsoft Excel, 2016 software. Data from all the experiments were expressed as the Mean ± SD (standard deviation of the mean) from three different replicates, and a P-value < 0.05 was regarded as statistically significant. A one-way ANOVA test was performed to analyse the difference between untreated and treated cells, followed by Tukey's multiple comparisons test. The P-values < 0.01 and < 0.001 were represented by (*) and (***) asterisk marks, respectively.

Results

Tri-spectroscopy analysis

UV-VIS spectrophotometry analysis

The UV-VIS spectra of the studied medicinal plants are summarized in (Table 1). The extracts revealed different band patterns in three clusters. Cluster I in the 200-280 nm range can be related to the electronic transition of the double bond electrons in olefinic compounds. Cluster II in the 290-350 nm wavelength range is attributed to the electronic transition from non-bonding electrons in carbonyl (C=O) and carboxyl (O=C-OH) groups. Finally, cluster III in the range of 380-480 nm corresponds to the electronic transition of several compounds, which contain the extension of conjugation from the aromatic compounds, as shown in (Fig. 3A).

FTIR spectra analysis

Infrared spectroscopy was used to identify the functional groups of the active components present in the extract based on the peak values in the infrared radiation region. When the extract was passed into the FTIR, the functional groups of the components were separated based on their peak ratio. The results of FTIR peak intensities and functional groups are shown in (Table 2). It was clear that the number of phenolic and or alcohol (O-H) gave a broad peak at around 3310-3370 cm^{-1}, while the number of aromatic rings (C=C) and amine (N-H) groups peaked at a peak of 1610-1650 cm^{-1} as shown in (Fig. 3B).

GC-MS analysis

Gas chromatography spectroscopy was used to identify the bioactive compounds found in the ethanolic extract of *A. judaica*. The active compounds, along with their concentration (peak area %), retention time (RT), molecular formula, area, and percentages (Table 3 and Fig. 3C), were summarized. The concentration percentages were recorded up to the 30 min mark.

Computational Analysis

Active site searching

The active binding sites of the protein were identified using the PyMOL server. The targeted receptor

Table —1 UV-VIS spectra peak characterization of *A. judaica* L.

Sample	Wavelength (nm)	Absorbance	Functional groups
A. judaica	231	1.95	Double bonds (olefinic and aromatic compounds)
	275	1.14	
	331	1.06	Non-bonding electron in (C=O) and (O=C-OH) groups
	411	0.11	Aromatic compounds

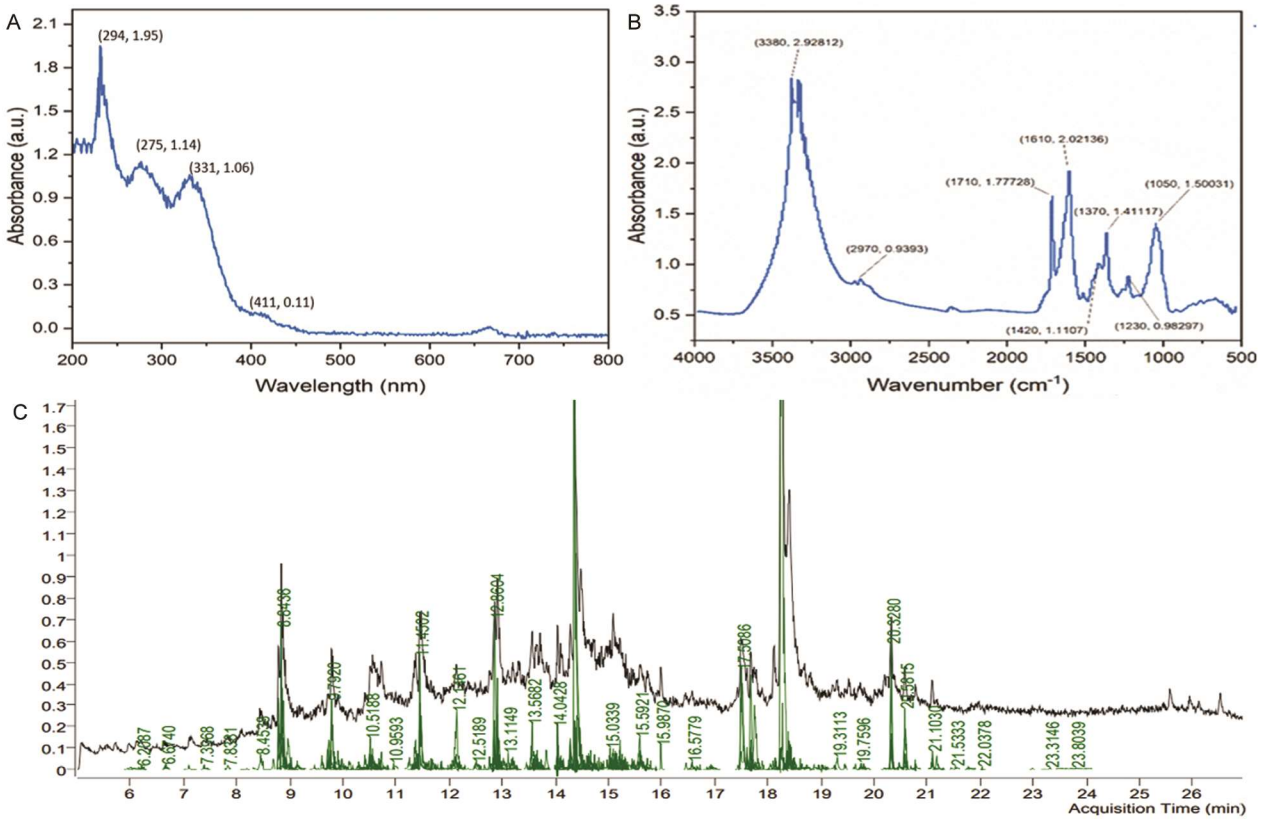

Fig. 3 —Tri-Spectroscopy analysis of *A. judaica* L. showing: (A) UV-VIS; (B) FTIR; and (C) GC-MS spectra

Table 2 —FTIR spectra peak characterization of *A. judaica* L.

Sample	Wave number (cm^{-1})	Intensity	Bond responsible
A. Judaica	2970	0.94	ν:C-H (Methyl & Methylene)
	1710	1.77	ν:C=O (Ester)
	1610	2.02	ν:C=C (Aromatic rings) δ: N-H (Amine)
	1420	1.11	δ:C-H (Saccharides)
	1370	1.41	δ:C-H (Ester)
	1230	0.98	ν:C-O (Ester, glycoside)
	1050	1.50	ν:C-O (Alcohol, acid, Saccharides)

ν: stretching*; δ:* bending

Table 3 —GC-MS spectra analysis of ethanolic extract of *A. judaica* L.

Peak	Compound retention time	Compound	Compound Formula	Compound Area	Compound (%)
1	6.0187	1H-Imidazolo[1,2-a] pyridine-6-carbonitrile, 2, 3-dihydro-7-methyl-1-(3,4-dimethylphenyl)-5-oxo-	$C_{17}H_{17}N_3O$	4667275.4	62.6
2	8.1953	5-(4-Bromobenzyl)-2-t-butyl-3-methyl-4-Oxoimidazolidine-1-carboxylic acid, allyl ester	$C_6H_{14}FO_2P$	4308913.0	57.9
3	8.6936	1,2-Benzenediol, O-(4-fluorobenzoyl)-O'-phenylacetyl	$C_{21}H_{15}FO_4$	7915306.7	51.5
4	9.6401	4,6-Bis(4-ethoxybenzylthio)-5-nitropyrimidine	$C_{22}H_{23}N_3O_4S_2$	2898864.7	64.6
5	11.3577	3-Trifluoromethylbenzoic acid, 4-nitrophenyl ester	$C_{14}H_8F_3NO_4$	12571848.6	67.7
6	11.6097	Benzamide, N-[4-(1H-1,3-benzimidazol-2-yl)-1, 2,5-oxadiazol-3-yl]-4-fluoro-	$C_{16}H_{10}FN_5O_2$	365327.3	53.4
7	11.8533	3-Phenyl-6-(4-nitrophenyl)-4H-(1,2,3) triazolo (1,5-d) (1,3,4) oxadiazin-4-one	$C_{16}H_9N_5O_4$	3656355.5	55.0
8	14.3598	1H-1,2,3-Triazole-4-carboxylic acid, 5-methyl-1-[4-(5-methyl-1,2,4-oxadiazol-3-yl)-1,2,5-oxadiazol-3-yl]-, ethyl ester	$C_{11}H_{11}N_7O_4$	549900197.0	57.3

(*Contd*.)

Table 3 —GC-MS spectra analysis of ethanolic extract of *A. judaica* L. *(Contd.)*

Peak	Compound retention time	Compound	Compound Formula	Compound Area	Compound (%)
9	14.6274	5-Nitrothiophene-2-carboxaldehyde picolinoylhydrazone	$C_{11}H_8N_4O_3S$	6464885.2	50.2
10	15.2212	Acetic acid, (dodecahydro-7-hydroxy-1,4b,8,8-tetramethyl-10-oxo-2(1H)-phenan threnylidene)-,2-(dimethyl amino)ethyl ester	$C_{24}H_{39}NO_4$	8974744.8	61.4
11	15.7238	Benzoic acid, 4-(diphenylphosphinoxido) methyl-, ethyl ester	$C_{22}H_{21}O_3P$	5362810.0	54.5
12	16.6706	Benzamide, 3-methyl-N-(2-bromophenyl)-	$C_{14}H_{12}BrNO$	2476691.7	52.5
13	17.7274	1,3-Benzenediol, O, O'-di(cyclopropanecarbonyl)-	$C_{14}H_{14}O_4$	10930669.6	55.3
14	17.7515	2-Benzofurancarboxylic acid, 7-methoxy-, (3,4,4-trimethyl-1,2-dioxetan-3-yl) methyl ester	$C_{16}H_9N_5O_4$	94887605.2	55.9
15	18.4049	N'-Hydroxy-3-methyl-2,4-dioxo-1-phenyl-1,2,3, 4-tetrahydropyrimidine-5-carboximidamide	$C_{12}H_{12}N4O_3$	25550520.7	52.5
16	18.4749	2-Amino-4,6-diphenylpyrimidine	$C_{16}H_{13}N_3$	2129674.1	63.0
17	18.4832	3a,6-Epoxy-3aH-isoindole, 1,2,3,6,7, 7a-hexahydro-6-methyl-2-phenyl-	$C_{15}H_{17}NO$	4979393.7	52.5
18	18.4913	4-Methoxy-N-methylphenylethylamine, pentafluorpropionyl	$C_{13}H_{14}F_5NO_2$	4532362.2	51.0
19	20.4748	2-Trifluoromethylbenzoic acid, 2-bromo-4-fluorophenyl ester	$C_{14}H_7BrF_4O_2$	6369042.3	50.6

Table 4 —Active site prediction of targeted protein caspase-3

Protein	Volume (SA)	Area (SA)	Resolution	Total AA residue in chain A	AA residues at predictive active site
Caspase-3	64.032	82.180	1.75	147	29

SA: Surface Area, AA: Amino Acids

Table 5 —Docking scores of four compounds selected from the *A. judaica* L.

S.N	Compounds	Pub Chem ID	Molecular Formula	Molecular Weigh	Binding Affinity (Kcal/mol)
1	Benzamide, N-[4-(1H-1,3-benzimidazol-2-yl)-1,2,5-oxadiazol-3-yl]-4-fluoro-	CID 135515055	$C_{16}H_{10}FN_5O_2$	323.28 g/mol	-9.2
2	3-Phenyl-6-(4-nitro- phenyl)-4H-(1,2,3) triazolo (1,5-d) (1,3,4) oxadiazin-4-one	CID 582339	$C_{16}H_9N_5o_4$	335.27 g/mol	-8.5
3	2-Benzofurancarboxylic acid, 7-methoxy-, (3,4,4-trimethyl-1,2-dioxetan-3-yl) methyl ester	CID 537428	$C_{16}H_{18}O_6$	306.31 g/mol	-7.2
4	2-Amino-4,6-diphenyl-pyrimidine	CID 619024	$C_{16}H_{13}N_3$	247.29 g/mol	-6.9

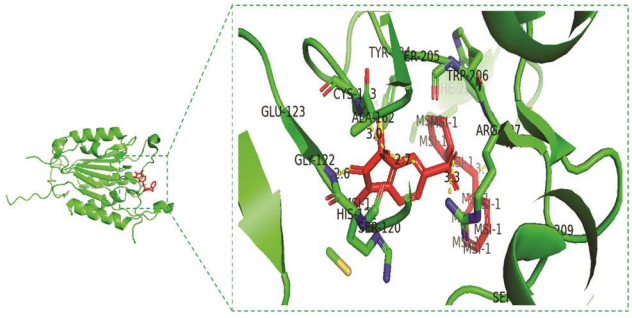

Fig. 4 —Caspase-3 protein active pocket showing the amino acid residue

showed most of the binding sites at the positions of ARG 207, CYS 163, GLY 122, SER 209, SER 120, SER 205, TYR 204, MET 61, HIS 121, ALA 162, and TRP 206 (Table 4 and Fig. 4).

MDanalysis

The bioactive chemicals from *A. judaica* were docked with the 1GFW receptor using the PyRx tools and AutoDock Vina, yielding binding affinity values ranging from -3.1 to -9.2. From a total of nineteen compounds, the compounds CID-135515055, CID-582339, CID-537428, and CID-619024 were selected. CID-1365597, CID-5303601, CID-583726, and CID-91714692 were selected for further molecular analysis as presented in (Table 5). Compound CID-135515055 of *A. judaica* showed many hydrogen bonds at ARG 207, ASN 208, SER 209, and PHE 250. The closet binding was observed in ARG 207 and SER 209 with distances of 2.53Å and 2.96Å. Additionally, two halogen bonds were observed at the positions of GLU 248 and SER 249 with distances 3.19Å and 3.68Å respectively (Fig. 5A). In compound CID-582339,

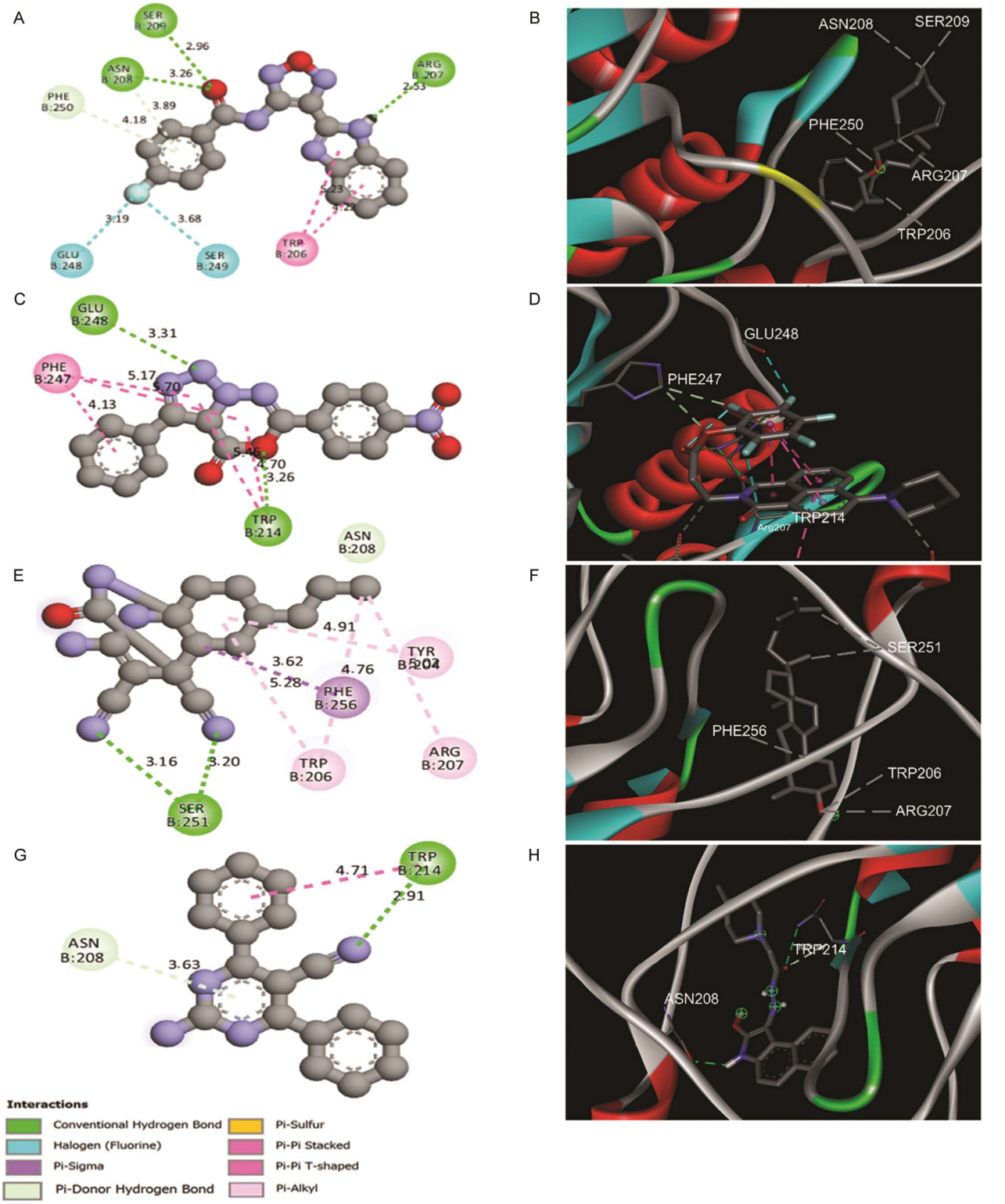

Fig. 5 —2D and 3D interactions between selected compounds from *A. judaica* extract and caspase-3: (A,B) CID-135515055 (benzamide, N-[4-(1H-1,3-benzimidazol-2-yl)-1,2,5-oxadiazol-3-yl] -4-fluoro-); (C,D) CID-582339 (3-phenyl-6-(4-nitro-phenyl) -4H-(1,2,3) triazolo(1,5-d) (1,3,4) oxadiazin-4-one); (E,F) CID-537428 (2-benzofurancarboxylic acid, 7-methoxy-, (3,4,4-trimethyl-1,2-dioxetan-3-yl methyl ester); and (G,H) CID-619024 (2-amino-4,6-diphenyl-pyrimidine)

hydrogen bonds were detected at the positions GLU 248 and TRP 214 with distances 3.31 Å and 3.26 Å respectively. Many hydrophobic links were formed at PHE with 4.13 Å, 5.17Å, and 5.70Å; TRP 214 with 4.70Å and 5.46Å of different distances (Fig. 5B). For compound CID-537428, many hydrophobic bonds were seen to form at TYR 204, TRP 206, ARG 207, and PHE 256 as PHE 256 and TYR 204 demonstrated the least distant values of 3.62Åand 4.91Å. Hydrogen bonds were detected at the position of SER251 with two distances of 3.20 Å and 3.16 Å (Fig. 5C). For compound CID-619024, some hydrogen bonds were detected at TRP214 with distances of 2.91Å and 4.71Å, ASN 208 with distance of 3.63Å (Fig. 5D).

ADMET pharmacokinetic analysis

According to Lipinski's rule of five[26], which limits molecular weight (MW) to < 500 g/mol, all the active compounds of *A. judaica* were detected within the recommended values. The hydrogen bond donor (HBD) enhances acidity, whereas the hydrogen bond acceptor (HBA) promotes basicity. The four selected compounds revealed an ideal range of HBD (0–5) and HBA (0–10) within the drug-like characteristics values. According to Lipinski's rule of five criteria, the log P value, which reflects the lipophilicity of a compound, was within the recommended (-2.0 – 6.5) range for all extracted compounds. The solubility of substances that directly affect absorption is measured by Log S. Most compounds of *A. judaica* showed moderate to well-qualified soluble degree, except for compounds 3, 4, and 11, which appeared to have poor solubility. Compounds 1, 2, 3, 10, 11, 12, 13, 16, 17, and 18 demonstrated the ability to cross the blood-brain barrier (BBB), while compounds 4,5,6,7,8,9,14,15, and 19 are unable to cross the BBB.Additionally, all the extracted compounds were good candidates for gastrointestinal absorption, except for compound 8, which showed lower absorption capacities. Finally, all the extracted bioactive compounds from *A. judaica* showed no cytotoxicity indications, as illustrated in (Table 6).

MD simulation analysis

Root Mean Square Deviation (RMSD) analysis

The Root Mean Square Deviation (RMSD) is used to assess the average change in displacement of selected atoms for a particular frame to the reference frame during molecular dynamics simulations. RMSD helps understand proteins' and ligands' structural conformation and stability over time. The comparison of the RMSD graphs for the simulations involving caspase-3 with four selected compounds from *A. judaica* revealed distinct trends in protein and ligand stability. The RMSD for compound CID-135515055 revealed initial instability but gradually stabilized, suggesting the ligand finds its binding position over time within the 1-3 Å range that indicates well-equilibrated systems (Fig. 6A). Meanwhile, compound

Table 6 —The pharmacokinetic properties of the extracted bioactive compounds from *A. judaica* L.

CID	MW	HBD	HBA	Log Po/W (SILICO S-IT)	Log S (SILICO S-IT)	BBB Permeability	GI absorption	Cytotoxicity
1	279.34	1	2	3.34	-5.03	Yes	High	No
2	168.15	0	3	1.22	-2.30	Yes	High	No
3	350.34	1	5	4.75	-7.14	Yes	High	No
4	381.49	1	3	4.65	-7.89	No	High	No
5	311.21	0	7	1.79	-4.85	No	High	No
6	323.28	0	6	1.65	-4.37	No	High	No
7	335.27	2	7	1.32	-4.53	No	High	No
8	305.25	2	8	-2.17	-1.86	No	Low	No
9	276.27	2	5	2.10	-2.79	No	High	No
10	405.57	1	5	3.51	-4.01	Yes	High	No
11	364.37	0	3	4.83	-8.24	Yes	High	No
12	290.16	0	2	4.54	-5.98	Yes	High	No
13	246.26	0	4	3.14	-3.48	Yes	High	No
14	285.34	2	3	1.59	-3.63	No	High	No
15	260.25	1	4	-0.91	-3.12	No	High	No
16	247.29	1	2	3.99	-6.33	Yes	High	No
17	227.30	1	1	3.29	-5.54	Yes	High	No
18	311.25	1	7	3.65	-4.84	Yes	High	No
19	363.10	0	6	5.04	-6.57	No	High	No

CID: Compound ID, MW: Molecular Weight, HBD: Hydrogen Bond Donor, HBA: Hydrogen Bond Acceptor, BBB: Blood-Brain Barrier, GI: Gastrointestinal.

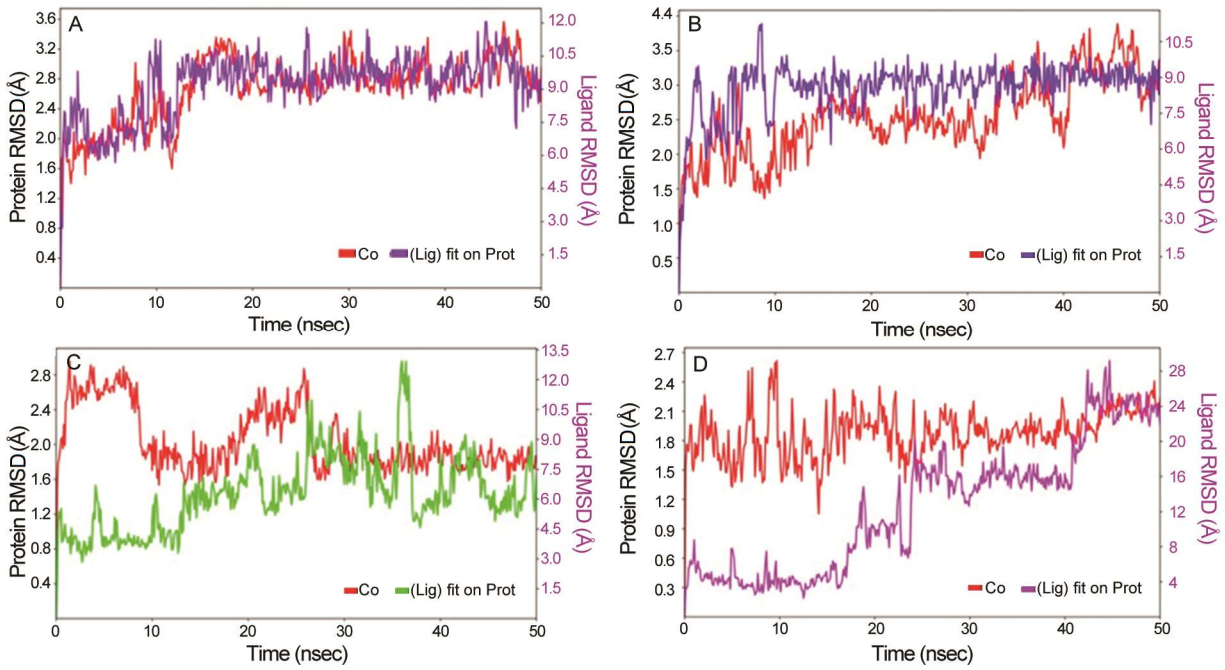

Fig. 6 — RMSD plot of apo-protein and ligand-protein complex of four selected compounds from *A. judaica*: (A) CID-135515055; (B) CID-582339; (C) CID-537428; and (D) CID-619024 over the period of 50 ns simulation

CID-582339 shows slightly higher fluctuations range from 0.7 to 3.0 Å but still within acceptable limits for small globular proteins (Fig. 6B). For compound CID-537428, the RMSD values fluctuate below 2.5 Å, suggesting stable behaviour through the simulation process (Fig. 6C). Also, compound CID-619024 remains relatively stable, fluctuating between 0.6 and 3.0 Å. This suggests a stable protein structure throughout the simulation (Fig. 6D).

Root Mean Square Fluctuation (RMSF) analysis

The Root Mean Square Fluctuation(RMSF) measures how much a protein's residues deviate from its average position. This shows regions that are flexible or rigid. Compound CID-135515055, the RMSF plot shows higher fluctuations at the terminal regions and stable secondary structure elements. The fluctuations in the loop regions are more pronounced. Compound interactions are marked, showing consistent contact throughout the simulation. This indicates that the ligand binding sites are stable despite the fluctuations in the loop regions (Fig. 7A). For compound CID-582339, moderate fluctuations, especially near active sites, were detected. This suggests a balance of flexibility (Fig. 7B). Compound CID-537428 has a flexibility profile like compound CID-582339, with some regions showing more mobility. This might help with necessary conformational changes for effective binding (Fig. 7C). Compared to other compounds, compound CID-619024 had the lowest RMSF value. This indicates a more rigid structure. The rigidity suggests it stabilizes caspase-3. This could positively impact its enzymatic activity if rigidity aligns with functional needs (Fig. 7D).

Secondary Structure Elements (SSE) analysis

The analysis of the secondary structure elements (SSE) from the molecular dynamic simulations of caspase-3 with four different ligands reveals variations in the protein's structural elements. These variations are key to understanding that ligand binding influences the protein's function and stability. Compound CID-135515055 percentage of alpha-helices is 21.79%. Beta-strands constitute 17.20%. The total SSE makes up 38.99% of the protein (Fig. 8A). For ligand CID-582339 exhibits a slightly higher helix content at 22.01% with 17.59% strands totalling 39.60% SSE. The increased helix percentage might imply that this ligand stabilizes certain alpha-helix regions. This could enhance the functional conformation of caspase-3 necessary for its enzymatic activity (Fig. 8B). Compound CID-537428 shows a secondary structure composition of 21.62% alpha-helices and 17.31% beta-strands. The total SSE coverage was 38.93%. This distribution suggests a balance of helices and strands, indicating that the ligand binding does not significantly disrupt the

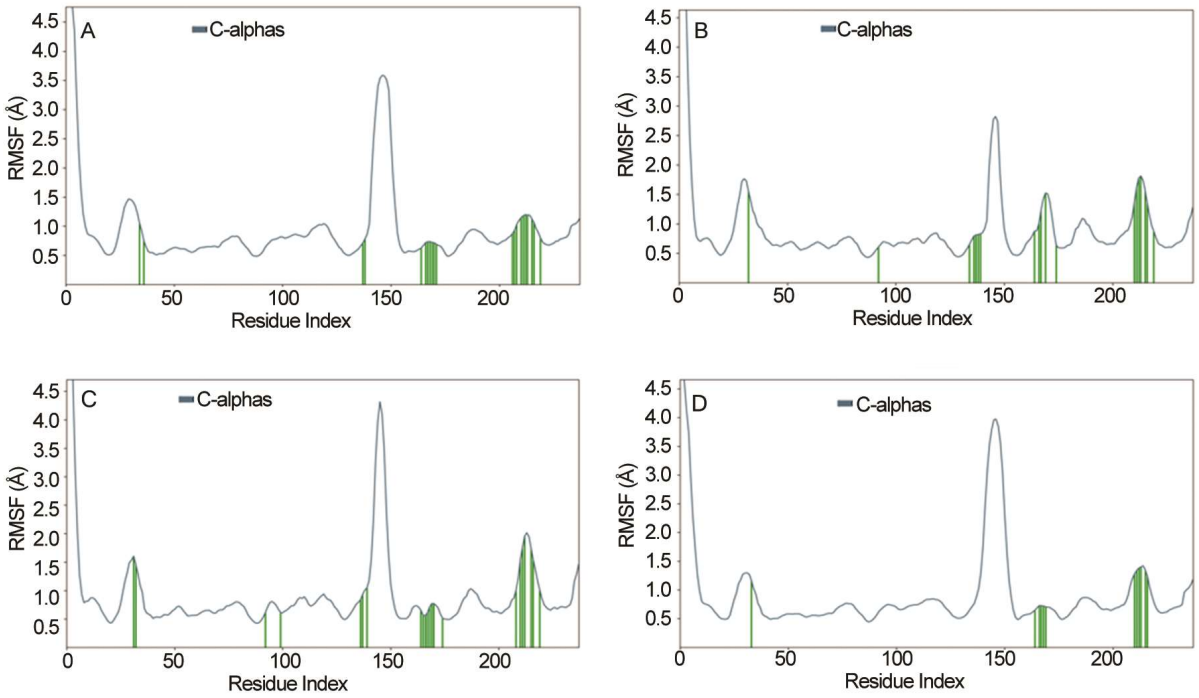

Fig. 7 — RMSF plot of apo-protein and ligand-protein complex of four selected compounds from *A. judaica*: (A) CID-135515055; (B) CID-582339; (C) CID-537428; and (D) CID-619024 over the period of 50 ns simulation

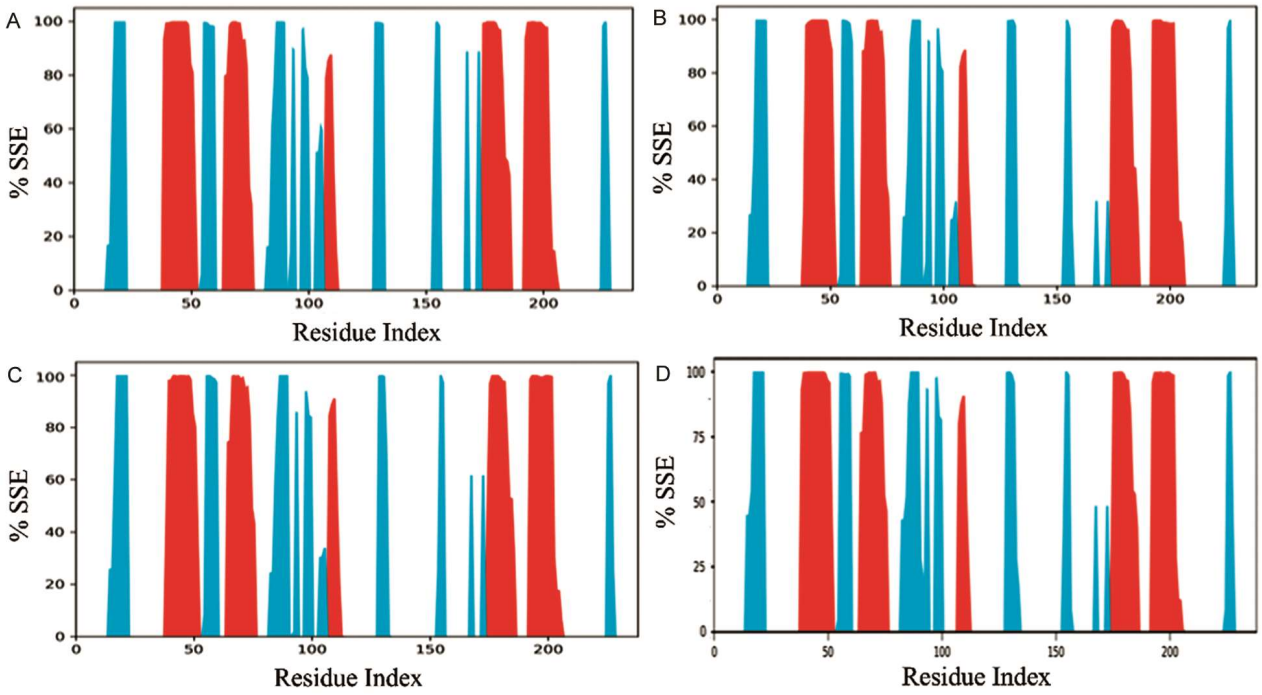

Fig. 8 — SSE plot of apo-protein and ligand-protein complex of four selected compounds from *A. judaica*: (A) CID-135515055; (B) CID-582339; (C) CID-537428; and (D) CID-619024 over the period of 50 ns simulation

protein's overall architecture (Fig. 8C). In contrast, compound CID-619024 presents a secondary structure composition with 21.62% helices, 17.49% strands and a total SSE of 39.11%. This profile indicates a slightly lower strand percentage compared to compounds CID-537428 and CID-582339, which could reflect subtle differences in how this ligand influences the stability and dynamics of caspase-3 (Fig. 8D).

Ligand Torsion Profile (LTP) analysis

The comprehensive ligand torsion profile (LTP) analysis across four simulations involving caspase-3 with different ligands reveals detailed interactions. These mechanisms adhere to specific geometric criteria necessary for effective binding. Compound CID-135515055 has moderate torsional activity. It is less dynamic and more flexible. It can adapt but within a semi-restricted range of conformations. This balance might make it suitable for various protein interactions while maintaining some structure (Fig. 9A). Compound CID-582339 follows a similar interaction pattern, distinguishing itself with a detailed timeline of contact points. This indicates frequent and diverse interactions across multiple protein residues and suggests dynamic engagement that could influence the protein's functional dynamics over the simulation (Fig. 9B). Compound CID-537428 shows strong hydrogen bonding. The

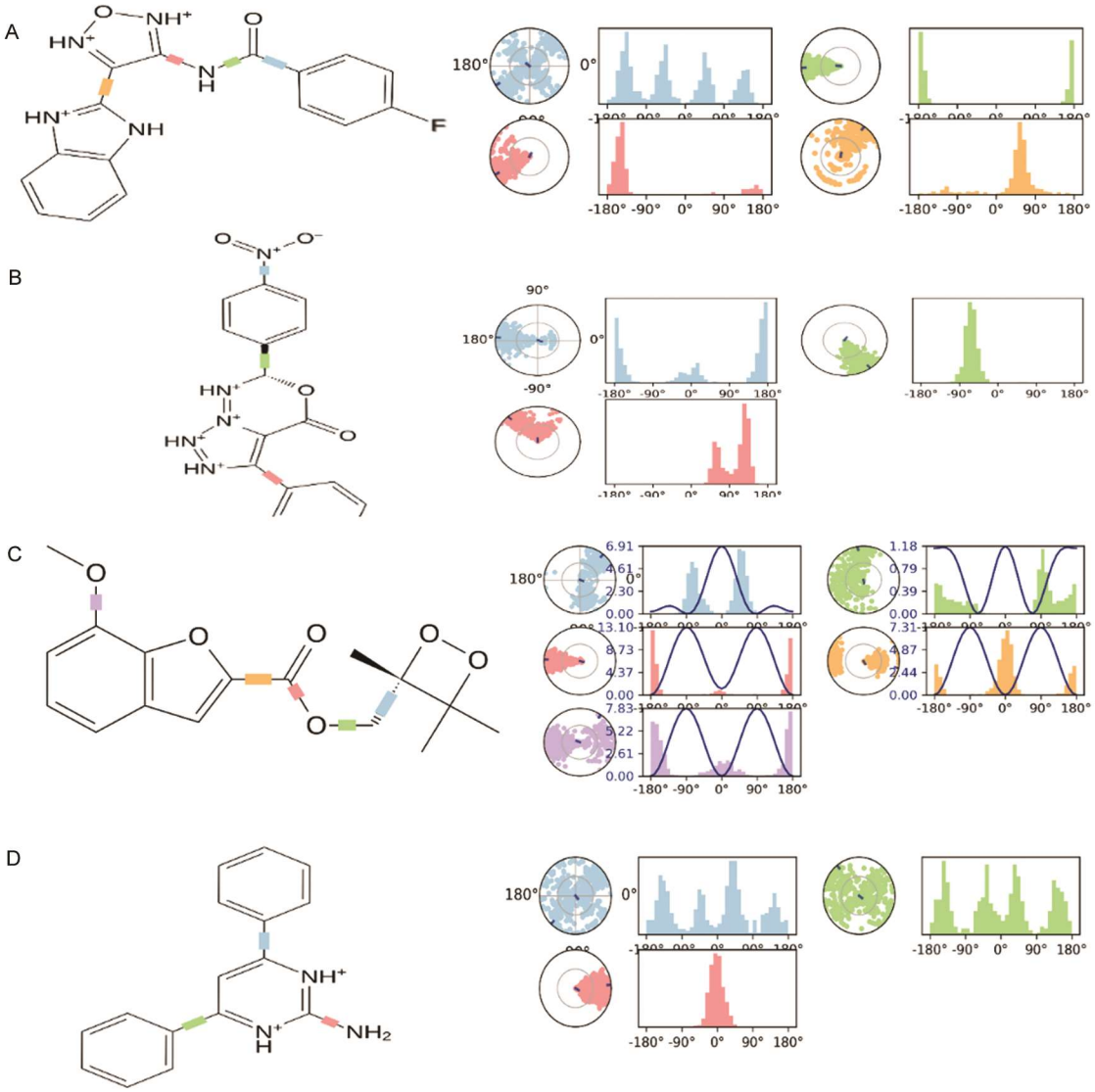

Fig. 9 — LTP plot of apo-protein and ligand-protein complex of four selected compounds from *A. judaica*: (A) CID-135515055; (B) CID-582339; (C) CID-537428; and (D) CID-619024 over the period of 50 ns simulation

distances are less than or equal to 2.5 Å. The angles are greater than or equal to 120° for optimal donor-acceptor alignment. This ligand also presents significant hydrophobic interactions. They include π-cation and π-π stacking within a range of 3.6 Å to 4.5 Å. There are ionic interactions and metal-ligand coordination within 3.7 Å and 3.4 Å, respectively. Water-mediated interactions play a crucial role. They feature slightly relaxed geometric criteria compared to standard hydrogen bonds (Fig. 9C). For compound CID-619024, an extensive array of hydrogen bonds was demonstrated strictly to adhere to the required geometric criteria. It also has well-defined hydrophobic and ionic interactions. The interaction dynamics over time are notably detailed. They show frequent interactions, suggesting possibly tighter or more stable binding than other ligands (Fig. 9D).

Acute toxicity analysis

To evaluate the cytotoxicity of extracted *A. judaica* bioactive constituents, we used an MTT assay to determine the cytotoxic effects of these components on the normal cell line HSF. Table 7 presented the inhibiting cytotoxic dose (IC_{50}) of treated HSF cells with DOX (Fig. 10A) and *A. judaica* extract (Fig. 10B). Our results revealed that normal cell line HSF treated with DOX could suppress cell growth at lower concentrations with IC_{50} of 1.135 ± 2.35 µg/mL as shown in treated cancer cells. Interestingly, the extracted compounds from *A. judaica* demonstrated nontoxic activity on cell growth of normal HSF cells with anIC_{50} value of 923.9 ± 5.33 µg/mL after twenty-four h. Moreover, to further confirm the anticancer efficiency of extracted *A. judaica* bioactive compounds, the SI values were calculated as presented in (Table 8). In all the cultured cancer cells, the extracted *A. judaica* compounds showed higher results (SI > 2) within the recommended ranges.

Anti-proliferative analysis

To investigate the anticancer activities of *A. judaica*extract compared to chemotherapeutic (DOX) as a positive control, the cytotoxicity of the extracted heterocyclic organic compounds was assessed by the 3-(4,5-dimethylthiazol 2-yl)-2,5-diphenyltetrazolium bromide (MTT) assay in four different cancer cell lines expressed oestrogen receptors, MCF-7 (breast adenocarcinoma), T47D (breast ductal carcinoma), MDA-MB-231 (TNBC), and HePG2 (hepatocellular adenocarcinoma). Table 9 presented the half-maximal inhibitory concentration (IC_{50}) values of the BC cell line MDA-MB-231 (Fig. 11A) and the LC HePG2 (Fig. 11B) treated with various concentrations of DOX. The cancer cells exhibited significant inhibition in cell viability at lower concentrations withIC_{50} values of 1.44 ± 0.04 µg/mL and 16.73 ± 2.09 µg/mL, respectively. On the other hand, in Table 7 displayed

Tabel 7 — IC_{50} values of normal cell line HSF treated with DOX and *A. judaica* L. for 24 h

Treatments	Normal cell line HSF
DOX	1.135±2.35
A. judaica L.	923.9 ± 5.33

Table 8 — SI values of ethanolic *A. judaica* L. extracted compounds calculated from experimental cancer cell lines

		Experimental cell lines				
		MCF-7	T47D	MDA-MB-231	HePG2	Recommended range
SI values	24 h	3.12	4.18	4.46	2.23	[1.96-51.3][21]
	48 h	4.85	5.32	8.87	2.84	

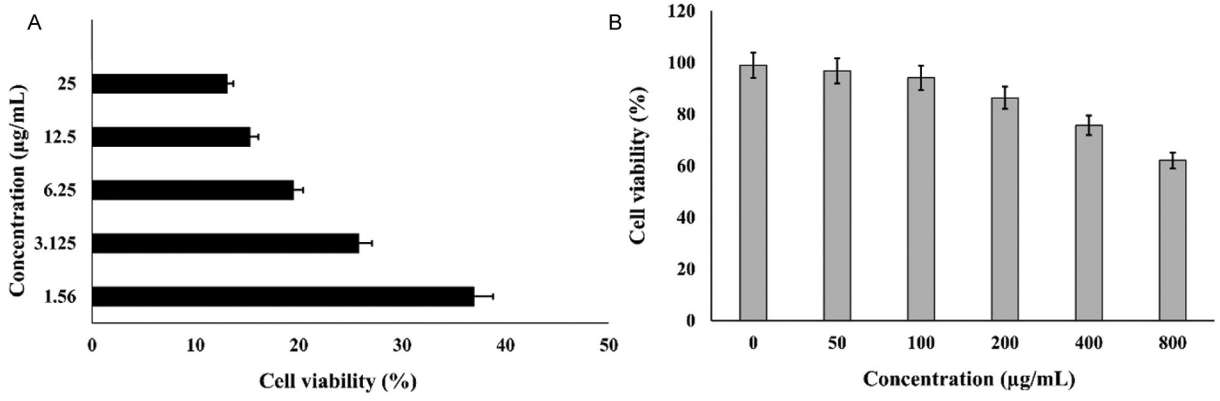

Fig. 10 —MTT assay showing the normal cell line HSF treated with various concentrations of (a) DOX; and (B) Extracted *A. judaica* compounds for 24 h.

Table 9—IC50 values of experimental cancer cell lines treated with DOX and the extracted *A. judaicaL.* compounds for 24 and 48 h

Treatments		Experimental cancer cell lines			
		MCF-7	T47D	MDA-MB-231	HePG2
DOX	24 h			1.44±0.04	16.73±2.09
A. judaica L.	24 h	167.5±3.58	179.7±3.32	152.7±3.18	363.09±4.73
	48 h	135.71±2.23	154.44±2.72	55.18±2.03	205.12±3.67

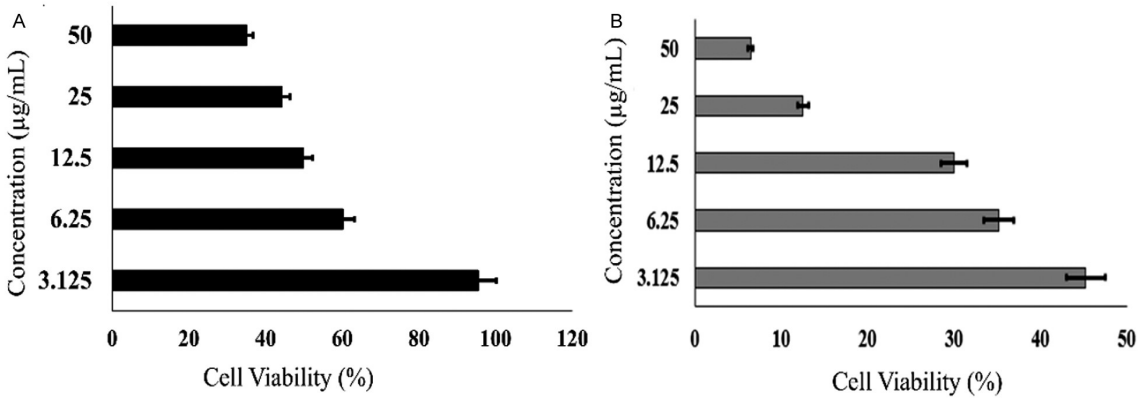

Fig. 11—MTT assay showing the cytotoxic effects of DOX at various concentrations on the growth of: (A) The BC cell line MDA-MB-231; and (B) The LC cell line HePG2 for 24 h

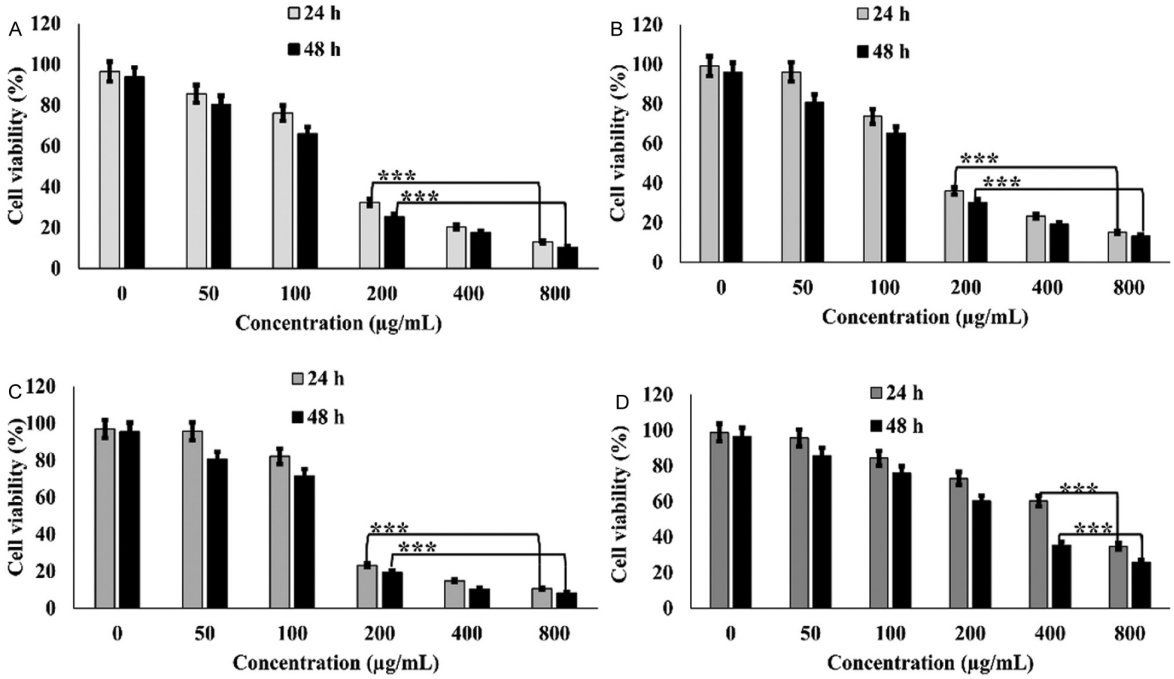

Fig. 12 —MTT assay showing the BC cell lines (A) MCF-7; (B) T47D; (C) MDA-MB-23; and the LC cell line (D) HePG2 for 24 and 48 h. One-way ANOVA followed by Tukey's post hoc test was used to compare the treatment groups and results were considered statistically significant when $p < 0.05$ in comparison with the control. The p-value < 0.001 represented by (***) asterisk mark. The Values are expressed as Mean ± SD of three independent experiments

show the half-maximal inhibitory concentration (IC_{50}) values of the BC cell lines MCF-7 (Fig. 12A), T47D (Fig. 12B), MDA-MB-231 (Fig. 12C), and the LC cell line HePG2 (Fig. 12D) medicated with various doses of extracted *A. judaica* compounds. Notably, a significant inhibition in cell proliferation was observed inMDA-MB-231 cells withIC_{50} values of 152.7 ± 3.18 µg/mL and 55.18±2.03 µg/mL; followed by MCF-7 withIC_{50} values of167.5 ± 3.58 µg/mL and 135.71 ± 2.23 µg/mL; T47D withIC_{50} values of 179.7 ±

3.32 µg/mL and 154.44 ± 2.72 µg/mL; and HePG2 withIC_{50} values of 363.09 ± 4.73 µg/mL and 205.12 ± 3.67 µg/mL, after 24 and 48 h, respectively.

Cell morphology analysis

Microscopical analysis of treated normal HSF cells treated with DOX demonstrated significant changes in losing cell texture at various lower concentrations (Fig. 13A). In contrast, cells treated with *A. judaica* extract showed no changes in morphological patterns. Cells still maintained their spindle-shaped characteristics (Fig. 13B). However, the BC cells MCF-7 (Fig. 14A), T47D (Fig. 14B), MDA-MB-231 (Fig. 14C), and LC cells (Fig. 14D) with DOX showed

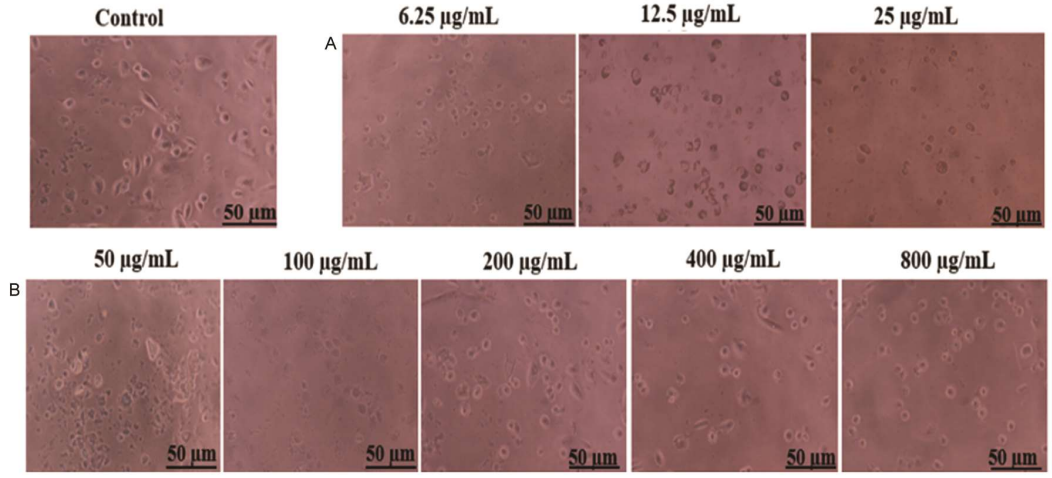

Fig. 13 — Microscopical examination of the normal cell line HSF treated with various concentrations of: (A) DOX; and (B) Extracted *A. judaica* compounds for 24 h. Images are captured with a LABOMED inverted microscope, (LABOMED®), at a magnification of 20x with a scale of 50 µM

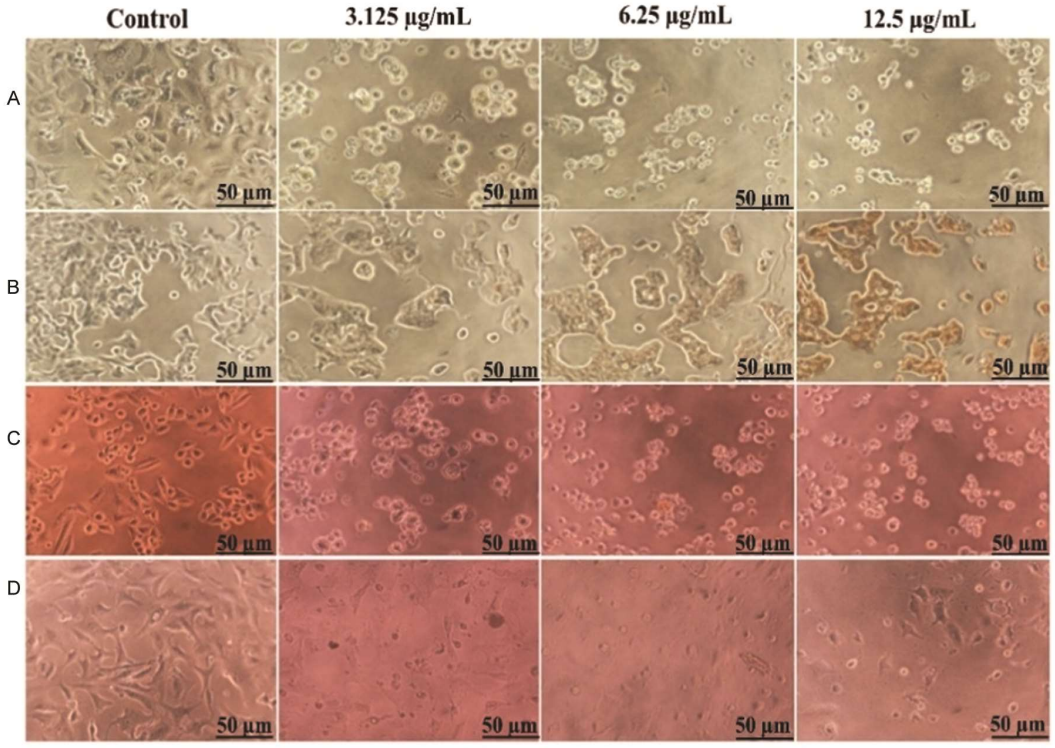

Fig. 14 —Microscopical examination of the BC cell lines (A) MCF-7; (B) T47D; (C) MDA-MB-231; and the LC cell line (D) HePG2, treated with various concentrations DOX for 24 h. Images are captured with a LABOMED inverted microscope (LABOMED®), at a magnification of 20x with a scale of 50 µM

more significant alterations in cell morphology at lower concentrations. In contrast, the BC cells MCF-7 (Fig. 15A), T47D (Fig. 15B), MDA-MB-231 (Fig. 15C), and LC cells (Fig. 15D) treated with *A. judaica* extract at a concentration of 200 µg/mL revealed few morphological changes, and most of the cells still retained their tumorigenic properties. At a concentration of 400 µg/mL, cancer cells began to lose their spindle shape and exhibit several cellular alternations, represented in cell shrinkage, contact inhibition, and loss of membrane integrity. At a higher concentration of 800 µg/mL, the morphological changes become more apparent, with a notable drop in viable cells and an increase in detaching cells. This suggests that the extracted bioactive compounds from *A. judaica* are causing cancer cells to undergo cell death.

ROS generation analysis

As previous results have observed, extracted *A. judaica* compounds could reduce cell viability in all cancer cells, particularly in metastatic TNBC cells MDA-MB-231 (of interest). Our subsequent evaluation was whether these compounds could over-accumulate ROS. The BC cell line MDA-MB-231 was labelled with Cell ROX Green to evaluate the generation of ROS. A higher fluorescence intensity percentage of 61.7% was determined in untreated (control) cells (Fig. 16A). In contrast, a lower percentage of 43.2% and 41.6% were detected in cells treated with DOX (Fig. 16B) and *A. judaica* extract (Fig. 16C), suggesting increased ROS levels, subsequently decreasing cell population.

Depolarization of MMP analysis

To further confirm the ROS generation, the BC cell line MDA-MB-231 was labelled with JC-1 protein to evaluate depolarized MMP. An increase in fluorescence intensity percentage from 39.7% in P1 to 45.5% in P2 was determined in untreated (control) cells (Fig. 17A), while a decrease percentage from 29.2% in P1 to 3.6% in cells treated with DOX (Fig. 17B), and from 32.9% in P1 to 8.2% in P2 in cells treated with *A. judaica* extract (Fig. 17C), respectively, following twenty-four h of treatment. A decrease in the ratio of aggregate red fluorescence (P1) to monomer blue fluorescence (P2) in treated cells indicates a loss in MMP compared to untreated cells.

Caspase-3 activation analysis

As previous results showed a decrease in MMP in cancer cells treated with *A. judaica* compared with

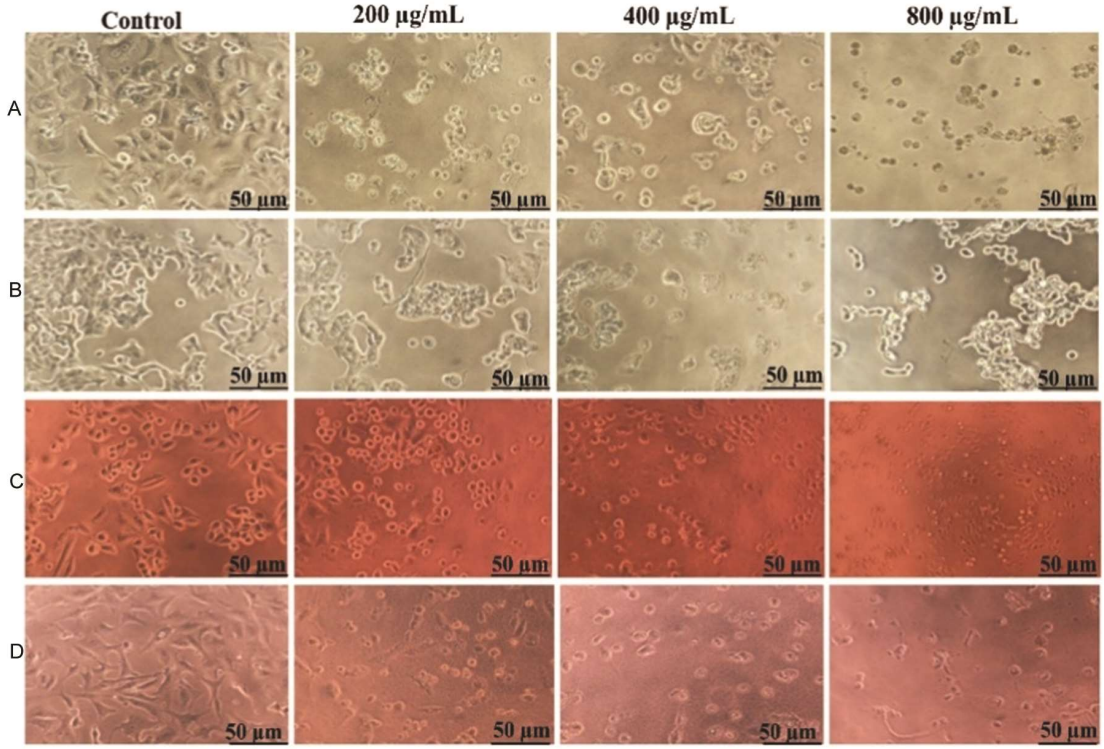

Fig. 15 — Microscopical examination of the BC cell lines (A) MCF-7; (B) T47D; (C) MDA-MB-231; and the LC cell line (D) HePG2, treated with various concentrations of the extracted *A. judaic* compounds for 48 h. Images are captured with a LABOMED inverted microscope (LABOMED®), at a magnification of 20x with a scale of 50 µM

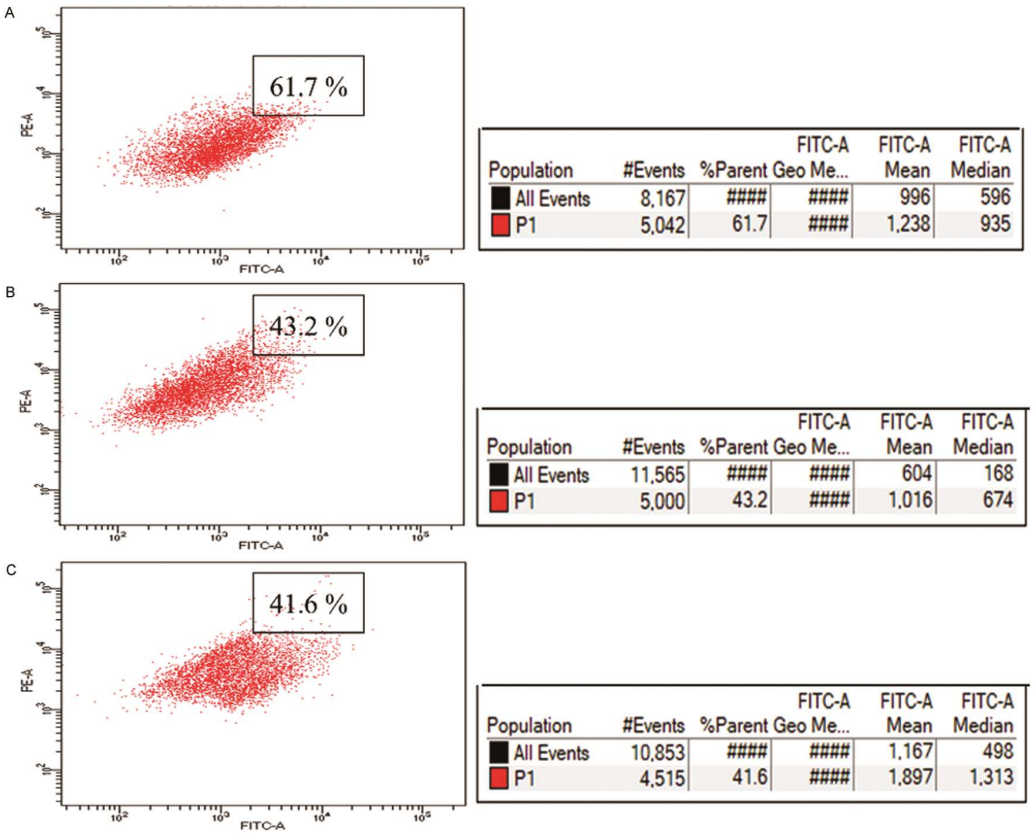

Fig. 16—The generation of ROS was evaluated by flow cytometry using CellRox green stain in the BC cell line MDA-MB-231: (A) Untreated (control) cells; treated with IC_{50} of (B) DOX (2 µg/mL); and (C) Extracted *A. judaica* compounds (100 µg/mL) for 24 h

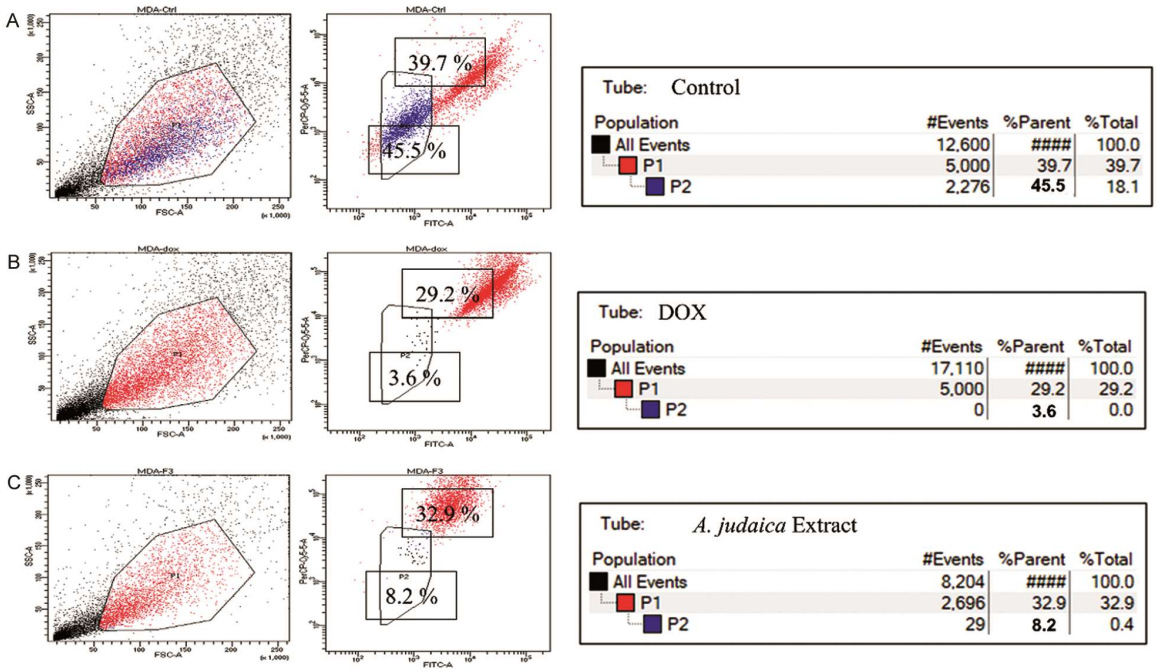

Fig. 17 —Measurement of depolarized MMP using JC-1 protein in the BC cell line MDA-MB-231: (A) Untreated (control) cells; treated cells with IC_{50} concentrations of (B) DOX (2 µg/mL); and (C) Extracted *A. judaica* compounds (100 µg/mL) for 24 h

DOX, we next investigated whether the extracted compounds could exhibit caspase-3-dependent mitochondrial activation. The dose-dependent increase in the activity of caspase-3 was determined in the BC cell line MDA-MB-231. CASPASE-Glo luminometric analysis of this protein revealed a highly significant increase ($p < 0.001$) in the level of the enzymes in treated BC cell line MDA-MB-231 with IC_{50} concentrations of DOX (2 µg/mL) and *A. judaica* extract (100 µg/mL), respectively (Fig. 18). These findings confirmed the previous data on anticancer activity of *A. judaica* that inhibited the cell growth of MDA-MB-231 cells.

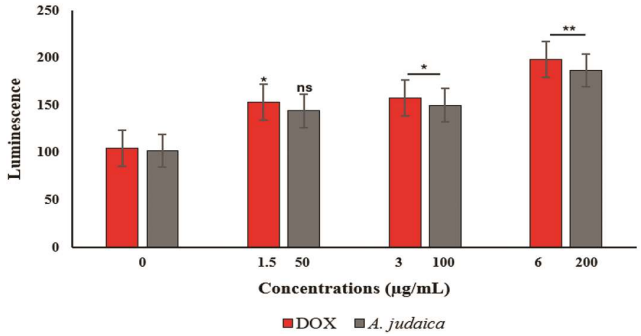

Fig. 18 — Caspase-3 activity was measured after 4 h of treatment with DOX and extracted *A. judaica* compounds at various IC_{50} concentrations in the BC cell line MDA-MB-231 using luminescence by a microplate reader. (p-value < 0.05) and (p-value < 0.001) was considered significant represented by (*) and (***) asterisk mark, respectively, and non-significant (ns)

Cell cycle analysis

Our subsequent investigation was whether the extracted *A. judaica* compounds could induce cell cycle compared to DOX.In comparison to untreated BC cell line MDA-MB-231 (control) (Fig. 19A) that showed cell population increasing from 60.2% in P1 (Sub-G0) to 93.4% in P2 (G0/G1) phases, in contrast to the cells treated with DOX (Fig. 19B) withIC_{50}concentration dose (2 µg/mL), showed a reduction in cells growth from 32.6% in P1 to 58.2% in P2. In contrast, cells treated with *A. judaica* extract (Fig. 19C) with IC_{50}concentration dose (100 µg/mL) exhibited inhibition percentages from 44.6% in P1 to 78.3% in P2.

Apoptosis and necrosis analysis

The data obtained from the analysis of the BC cell line MDA-MB-231 treated with DOX and *A. judaica* extract for twenty-four h and stained with annexin V/PI for flow cytometer study confirmed the previous process of cell cycle induction through the mode of cell death and apoptosis. The scatter profile of Annexin FITC and PI stain suggested that 61.5% of

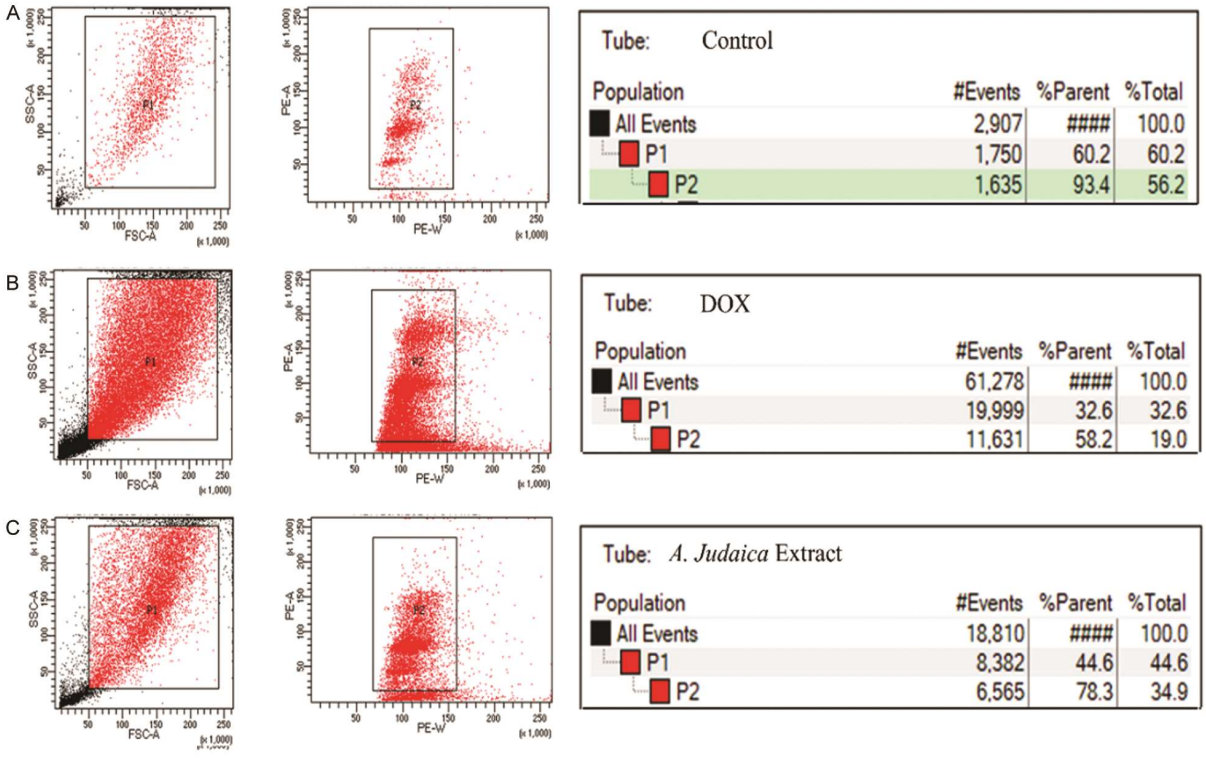

Fig. 19 —Flow cytometric analysis of cell cycle arrest in MDA-MB-231 cell showing (A) Untreated (Control) cells; cells treated with IC50 concentrations of (B) DOX (2 µg/mL); and (C) Extracted *A. judaica* compounds (100 µg/mL) for 24 h

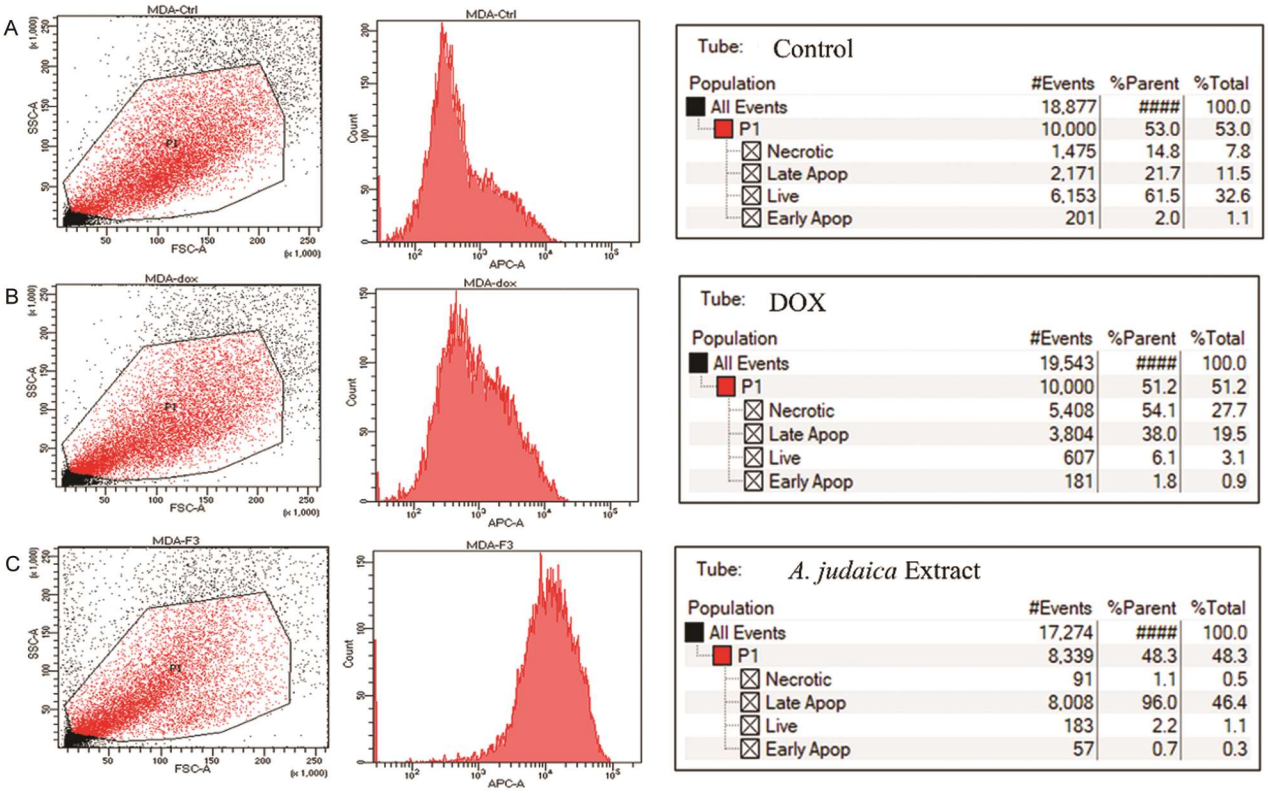

Fig. 20—Detection of apoptosis was evaluated using annexin V-FITC in MDA-MB-231 cells showing (A) Untreated (Control) cells; cells treated with IC50 concentrations of (B) DOX (4 µg/mL); (C) Extracted *A. judaica* compounds (100 µg/mL) for 24 h

cells were viable in the untreated (control) cell population (Fig. 20A) compared to 6.1% and 2.2% in treated cells with DOX (Fig. 20B) and *A. judaica* extract (Fig. 20C). However, an early apoptotic cell population of 1.8% and 0.7% and late apoptotic cell population of 38% and 96% in cells treated with IC_{50}concentrations of DOX (2 µg/mL) and *A. judaica* (100 µg/mL), respectively. Additionally, the cells treated with DOX showed a necrotic cell population of 54.1% compared to 1.1% and 14.8% in treated cells with *A. judaica* extract and untreated cells, respectively. We found that treated MDA-MB-231 cells at IC_{50} concentrations of *A. judaica* extract, compared to DOX, exhibited a slight increase in the early apoptotic cell population with an increment in the late apoptotic cell population.

Discussion

Chemotherapeutics have become a key agent in breast cancer treatment, and despite their side effects, they remain the first choice for patients to control the development of the disease. The different regimes of chemo-and-radiotherapeutic doses target cancer cells and the surrounding healthy cells, resulting in increasing body toxicity and aging acceleration. Therefore, we employed a green medicine strategy to prevent or at least inhibit the growth and metastasis of breast and liver cancer cells. This study used trispectroscopy UV-VIS, FTIR, and GC-MS analytical techniques to identify the main bioactive components in the aromatic herb, *Artemisia judaica* (L.). The fresh leaves were macerated in a pure ethanolic solution as a safe polar solvent in addition to its distinctive properties of attracting non-polar phytochemical constituents such as phenolics, flavonoids, and fatty acids[27]. The non-destructive FTIR spectra method provides crucial information about the chemical composition of materials; samples with higher peak intensities indicate stronger absorption of infrared radiation at specific frequencies, which correlates with the presence and concentration of certain functional groups[28]. The obtained extraction from *A. judaica* was characterized majorly by the presence of aromatic organic compounds (2.66), phenolics (1.59) and esters (1.77), suggesting the important role of the presence of aromatic organic compounds in combination with phenolics that possess antioxidant and anti-proliferative activities through the regulation of oxidative stress[29].

Moreover, the GC-MS profile of *A. judaica* crude extract was characterized by novel heterocyclic organic compounds. Benzamide, a class of enzymes known as histone deacetylases (HDACs), removes acetyl groups from histones, causing chromatin condensation and transcriptional inhibition. It has high cytotoxic effects against various cancer cells that cause cell cycle arrest, activate several pro-apoptotic genes, and have a strong tolerance to drugs in breast cancer[30]. Oxadiazine, a heterocyclic compound, has potent anti-proliferative activity, induces apoptosis[31], and inhibits mitochondria membrane potential[32]. Benzofuran-carboxylic acid, another heterocyclic compound extracted from *A. judaica* extract, could enhance the hypoxic tumour microenvironment through the HIF-1α/VEGF pathway[33]. Drugs-based pyrimidine displayed potent inhibitory effects on the proliferation, invasion, and migration of TNBC through blocking FAK-mediated signalling pathways[34].

Preliminary assessment of biomolecules using modern, sophisticated technologies can forecast the compounds' efficacy and reduce the time and expense of finding new treatments[35]. Molecular docking and computational pharmacokinetic analysis were utilized to predict the binding affinities, degree of solubility, and cytotoxicity of extracted *A. judaica* compounds. Our initial results revealed that the bioactive compounds exhibited a greater affinity for binding to the caspase-3 protein. This may be attributed to many hydrogen and hydrophobic bonds with the specific receptor. According to Patil *et al*.[36], hydrophobic and hydrogen bonding can change binding affinity and medication efficacy while being essential in stabilizing the ligands at the active site. Halogen bonds also play a critical role in enhancing drug-target binding affinity and adjusting ADMET properties, according to Xu *et al*.[37]. Besides intermolecular bonding, pharmacokinetics and ADMET characteristics are important factors in drug development. According to a recent study, physicochemical properties like lipophilicity and molecular weight can improve compound safety and efficacy and lead to positive therapeutic outcomes[38].

However, since low MW chemicals are likely to be highly absorbed, disseminated, and transported across membranes, this can strongly correlate with solubility, cellular membrane permeability, and passive diffusion. On the other hand, because they cannot pass through cellular membranes, high MW molecules have poor absorption along the gastrointestinal tract. According to Lipinski's criterion, all the isolated compounds from *A. judaica* have recommended values [39]. HBA and HBD are additional important factors; molecules with limited permeability and solubility[40] may cause low oral bioavailability. Adding hydrogen bond acceptors might maximize molecules' aqueous solubility, increasing the compounds' bioavailability[41]. The extracted compounds demonstrated moderate to well-qualified solubility, which increased their bioactivity and efficiency as potential drug candidates. Remarkably, it was found that the active molecules of *A. judaica* showed high binding affinities and interactions with the 1GFW receptor by the formation of hydrogen bonds at the amino acid residues GLU 248 TRP 214, ARG 207, ASN 208, and SER 209. While GLU contributes through ionic contacts and SER participates in hydrogen bonding, ARG exhibits numerous interactions since it has four hydrogen-bond donors, which makes it essential for compound stabilization.

By enabling focused, quick, and simple research, bioinformatic, validatory algorithms, and computer simulation modelling tools contribute significantly to the alluring appeal of nanoparticles and nano drug formulations. Recent research has emphasized the significance of RMSF analysis in comprehending protein-compound interactions. These interactions impact drug design. RMSF data can predict the functional effects of ligand binding on protein dynamics[42]. In contrast to other compounds that showed less consistent binding, our results revealed that the compounds CID-135515055 and CID-537428 from *A. judaica* exhibited the most stable binding trends with caspase-3, indicating potential stability and lower RMSD and RMSF values. Protein-compound docking for high-quality protein structure is a well-known technique for limiting the number of potential treatments for experimental testing in drug discovery and development, and the protein is often thought of as entirely or partially stiff[43].

Furthermore, the SSE of chemicals is essential for protein folding and structure. The selected ligands' secondary structure data revealed that each interacts with caspase-3 differently. Its helical and strand components are slightly impacted differently by this special coupling. These variations are crucial for comprehending how the substance can affect protein function, as shifts in the percentages of helices and strands may be associated with adjustments in substrate binding, regulatory processes, or enzymatic activity. In molecular dynamics simulations, ligands—chemical

compounds containing a single rotatable link between each compound—move without breaking their bonds. Once the motion occurs, the rotamer rotates within the compound's single links[44].Also,the LTP can provide information on the compound torsion strength based on theoretical calculations and the target location during the simulation phase[45]. In general, the selected compounds showed good stability and compactness interactions with caspase-3 compared to other compounds, suggesting the importance of the linking contacts of hydrogen and hydrophobic bonds, ionic and water-mediated interactions that maintain compound flexibility over time.

The *In vitro* assays have demonstrated that the extracted heterocyclic compounds from *A. judaica* possess anticancer effects in various oestrogen-sensitive cancer cells. We found that cancer cells treated with DOX showed high inhibition in cell viability by 85% at lower concentrations in the BC cell line MDA-MB-231, the LC cell line HePG2, and normal cell line HSF. In contrast, there is a higher significant reduction in cell growth in MDA-MB-231 cells, followed by cancer cells MCF-7, T47D, and HePG2 cells treated with higher concentrations of *A. judaica* extract, respectively, with no cytotoxic effects on the normal HSF cells with (SI > 2). These findings align with previous studies[46,47], which found that different *A. judaica* extracts significantly reduce breast cancer cell proliferation and progression. We suggest that heterocyclic compounds such as benzamide (C_7C_7NO), oxadiazine ($C_3H_4N_2O$), benzofuran (C_8H_6O), and pyrimidine ($C_4H_{44}N_2$) in *A. judaic* extract may inhibit the cell growth and proliferation.

Free radicals and ROS are the most mutagenic factors that accelerate cancer cell progression. This can enhance genomic alterations and DNA damage and facilitate the immortality of malignant cells[57]. Several signalling pathways associated with increased ROS levels support cancer cell invasion and metastasis[48]. We found that the concentration-dependent stimulation of ROS production in the BC cell line MDA-MB-231 upon treatment with the extracted *A. judaica* compounds was to the extent of untreated cells and DOX, respectively. The antioxidant molecules in the heterocyclic organic compounds may bind free radicals and increase ROS levels by neutralizing toxic oxidative substances. Similar findings confirmed that the antioxidant activity of this species can reduce the effect of oxidative stress[49].

We evaluated the extracted heterocyclic compounds' antioxidant activity by measuring the MMP disruption. The MMP plays a key role in the initiation of the apoptosis process. Therefore, we measured the MMP to examine these compounds on membrane potential stability. In the untreated cells, we observed red fluorescence emitted by JC-1 aggregates, whereas JC-1 monomers increased the intensity of blue fluorescence. In contrast, the BC cell line MDA-MB-231 treated with DOX and *A. judaic* extract decreases MMP intensity. This confirmed our previous results of ROS generation, as the increased levels of ROS lead to disruption of the MMP and subsequent release of cytochrome-c and activation of pro-caspases. Similar extracted compounds from *A. judaica* species exhibited antioxidant activity against free radicals that disrupt MMP[50].

The Caspases family are essential protease proteins that maintain homeostasis and develop cellular morphology by regulating cell death and inflammatory processes[51]. Caspase-3 plays a key role in various signalling pathways and has recently linked with cell death pathways in pathological diseases such as inflammation and cancer[52]. The generation of ROS that led to the initiation of MMP disruption upon treatment of MDA-MB-231 cells with *A. judaica* resulted in an increase in caspase-3 production compared to DOX and untreated cells, suggesting the activation of the apoptotic mechanism through the intrinsic pathway of apoptosis. Younes *et al*.[53] found that methanolic extract induced apoptosis through activation of caspase-3 in the breast cancer cell line MCF-7.

Upon activation of caspase-3 through triggers of the mitochondrial membrane, the cell cycle of the BC MDA-MB-231 cells treated with *A. judaica* is arrested at the G0/G1 phase through a DNA fragmentation-dependent mechanism, confirming the preponderant activity of extracted heterocyclic compounds that reduced cell viability and altered nuclear morphology. The results obtained from flow cytometric analysis of Annexin V/PI-stained BC MDA-MB-23 cells treated with *A. judaica* confirmed the cell death through the induction of apoptosis. Treated cells with a half-inhibition concentration of *A. judaica* resulted in a higher increase in a late apoptotic cell population with a slight decrease in an early apoptotic cell population with lower percentages of necrotic cells to the extent of cells treated with DOX. These findings align with previous studies that showed the anticancer activity of *Artemisia* species by increasing the apoptotic cell population by activating the mitochondrial apoptosis pathway[54]. We suggest

that the extracted heterocyclic organic compounds from *A. judaica* may have the ability to induce the caspase-3-dependent mitochondrial pathway through inhibition of cell proliferation, invasion, and metastasis. Similar organic compounds (Cholesta-8,24-dien-3-ol) showed potential anticancer activity against different hormonal-dependent cancer cells through activating the intrinsic caspase-3 pathway[55].

Conclusion

The results revealed that the extracted heterocyclic organic components from *A. judaica* leaves contain a variable interesting ingredient; using the GC-MS, benzamide, oxadiazine, benzofuran, and pyrimidine compounds were characterized. These compounds demonstrated significantly higher anticancer activity against the TNBC cell line MDA-MB-231 than oestrogen-sensitive cancer cell lines MCF-7, T47D, and HePG2, respectively. This may be attributed to atoms like nitrogen interacting with the major and minor grooves of DNA and the resulting inhibition of DNA replication. The biomolecular analysis also confirmed these compounds' potent binding affinities and stability when interacting with caspase-3 protein. The extracted compounds could inhibit the intrinsic apoptotic caspase-3 pathway by reducing cell proliferation and inducing cell cycle and apoptosis of the metastatic TNBC MDA-MB-231 cells by increasing ROS and disrupting MMP depolarization via activating the caspase-3-dependent mitochondrial pathway with no toxic effects on normal HSF cells and to extend cells treated with DOX. The anticancer activities of *A. judaica* extract may be attributed to the presence of binding heterocyclic compounds that may enhance the antagonist effects against oestrogen receptors in the metastatic TNBC MDA-MB-231 cells.

Acknowledgement

The authors gratefully acknowledge for financial support under grant no. G:653-130-1443, provided by King Abdulaziz University-Institutional Funding Program for Research and Development, Ministry of Education, Kingdom of Saudi Arabia.

Conflicts of interest

All authors declare no conflict of interest.

References

1 Zhu Y, Xie N, Chai Y, Nie Y, Liu K, Liu Y & Zhang C, Apoptosis induction: a sharp edge of berberine to exert anti-cancer effects, focusing on breast, lung, and liver cancer. *Front Pharmacol,* 13 (2022) 803717.

2 Brasó-Maristany F, Paré L, Chic N, Martínez-Sáez O, Pascual T, Mallafré-Larrosa M, Schettini F, González-Farré B, Sanfeliu E, Martínez D, Galván P, Barnadas E, Salinas B, Tolosa P, Ciruelos E, Carcelero E, Guillén C, Adamo B, Moreno R, Vidal M, Muñoz M & Prat A, Gene expression profiles of breast cancer metastasis according to organ site. *Mol Oncol,* 16 (2022) 69.

3 Bergin AR & Loi S, Triple-negative breast cancer: recent treatment advances. *F1000Res,* 8 (2019) F1000 Faculty Rev-1342.

4 Brodt P, Role of the microenvironment in liver metastasis: from pre- to prometastatic niches. *Clin Cancer Res,* 22 (2016) 5971.

5 Moats RK & Ramirez VD, Electron microscopic visualization of membrane-mediated uptake and translocation of estrogen-BSA: colloidal gold by Hep G2 cells. *J Endocrinol,* 166 (2000) 631.

6 Chen JQ & Yager JD, Estrogen's effects on mitochondrial gene expression: mechanisms and potential contributions to estrogen carcinogenesis. *Ann N Y Acad Sci,* 1028 (2004) 258.

7 Naeem M, Iqbal MO, Khan H, Ahmed MM, Farooq M, Aadil MM, Jamaludin MI, Hazafa A & Tsai WC, A review of twenty years of research on the regulation of signaling pathways by natural products in breast cancer. *Molecules,* 27 (2022) 3412.

8 Bora KS & Sharma A, The genus *Artemisia*: a comprehensive review. *Pharm Biol,* 49 (2011) 101.

9 Mamatova AS, Korona-Glowniak I, Skalicka-Woźniak K, Józefczyk A, Wojtanowski KK, Baj T, Sakipova ZB & Malm A, Phytochemical composition of wormwood (*Artemisia gmelinii*) extracts in respect of their antimicrobial activity. *BMC Complement Altern Med,* 19 (2019) 288.

10 Bisht D, Kumar D, Kumar D, Dua K & Chellappan DK, Phytochemistry and pharmacological activity of the genus *Artemisia*. *Arch Pharm Res,* 44 (2021) 439.

11 Feng S, Zha Z, Wang Z, Yang P, Wu J, Li X & Liu Y, Anticancer activity of oleiferoside B involving autophagy and apoptosis through increasing ROS release in MCF-7 and SMMC-7721 cells. *Nat Prod Res,* 35 (2021) 4865.

12 Doley J, Singh LV, Kumar GR, Sahoo AP, Saxena L, Chaturvedi U, Saxena S, Kumar R, Singh PK, Rajmani RS, Santra L, Palia SK, Tiwari S, Harish DR, Kumar A, Desai GS, Gupta S, Gupta SK & Tiwari AK, Canine parvovirus type 2a-induced apoptosis in MDCK involves both extrinsic and intrinsic pathways. *Appl Biochem Biotechnol,* 172 (2014) 497.

13 Liu X, Wang J, Lu C, Zhu C, Qian B, Li Z, Liu C, Shao J & Yan J, The role of lysosomes in BDE-47-mediated activation of the mitochondrial apoptotic pathway in HepG2 cells. *Chemosphere,* 124 (2015) 10.

14 Bennour N, Mighri H, Eljani H, Zammouri T & Akrout A, Effect of solvent evaporation method on phenolic compounds and the antioxidant activity of *Moringa oleifera* cultivated in Southern Tunisia. *S Afr J Bot,* 129 (2020) 181.

15 Patle TK, Shrivas K, Kurrey R, Upadhyay S, Jangde R & Chauhan R, Phytochemical screening and determination of phenolics and flavonoids in *Dilleniapentagyna* using UV-Vis and FTIR spectroscopy. *Spectrochim Acta A Mol Biomol Spectrosc,* 242 (2020) 118717.

16 Shahmoradi R, Talebibahmanbigloo N, Javidparvar A, Bahlakeh A & Ramezanzadeh B, Adsorption and inhibition effects of cellulose and lignin compounds extracted from agricultural waste on mild steel corrosion in HCl solution. *J Mol Liq,* 304 (2020) 112751.

17 Hago S, Lu T, Alzain AA, Abdelgadir AA, Yassin S, Ahmed EM & Xu H, Phytochemical constituents, in vitro anticancer activity and computational studies of *Cymbopogon schoenanthus*. *Nat Prod Res,* 5 (2024) 1.

18 Yahaya MAF, Bakar ARA, Stanslas J, Nordin N, Zainol M & Mehat MZ, Insights from molecular docking and dynamics on the potential of vitexin as an antagonist against LPS-induced microglial activation in neuroinflammation. *BMC Biotechnol,* 21 (2021) 38.

19 Kamiloglu S, Sari G, Ozdal T & Capanoglu E, Guidelines for cell viability assays. *Food Front,* 1 (2020) 332.

20 Plumb JA, Cell sensitivity assays: the MTT assay. *Methods Mol Med,* 88 (2004) 165.

21 Indrayanto G, Putra GS & Suhud F, Validation of in vitro bioassay methods: application in herbal drug research. *Profiles Drug Subst Excip Relat Methodol,* 46 (2021) 273.

22 Qi LF, Xu ZR, Li Y, Jiang X & Han XY, In vitro effects of chitosan nanoparticles on proliferation of human gastric carcinoma MGC803 cells. *World J Gastroenterol,* 11 (2005) 5136.

23 Wang HQ, Sun XB, Xu YX, Zhao H, Zhu QY & Zhu CQ, Astaxanthin upregulates heme oxygenase-1 via ERK1/2 pathway and protects SH-SY5Y cells from β-amyloid-induced cytotoxicity. *Brain Res,* 1360 (2010) 159.

24 Fried J, Perez AG & Clarkson BD, Flow cytofluorometric analysis of cell cycle distributions using propidium iodide: properties and mathematical analysis. *J Cell Biol,* 71 (1976) 172.

25 Kumar R, Saneja A & Panda AK, Annexin V-FITC/propidium iodide-based method for detecting apoptosis in non-small cell lung cancer cells. In: *Lung Cancer: Methods and Protocols,* 213 (2021) 223.

26 Petit J, Meurice N, Kaiser C & Maggiora G, Softening the rule of five: where to draw the line? *Bioorg Med Chem,* 20 (2012) 5343.

27 Abubakar AR & Haque M, Preparation of medicinal plants: basic extraction and fractionation procedures for experimental purposes. *J Pharm Bioallied Sci,* 12 (2020) 1.

28 Al-Kadhemy MFH & Alwaan EM, FTIR spectrum of laser dye fluorescein-doped polymer PMMA films. *Res Rev Pure Life Sci,* 3 (2012) 102.

29 Lin D, Xiao M, Zhao J, Li Z, Xing B, Li X, Kong M, Li L, Zhang Q, Liu Y, Chen H, Qin W, Wu H & Chen S, An overview of plant phenolic compounds and their importance in human nutrition and management of type 2 diabetes. *Molecules,* 21 (2016) 1374.

30 Movafagh S & Munson A, Histone deacetylase inhibitors in cancer prevention and therapy. In: *Epigenetics of Cancer Prevention,* Academic Press, (2019) 75.

31 Voráčová K, Hájek J, Mareš J, Urajová P, Kuzma M, Cheel J, Villunger A, Kapuscik A, Bally M, Novák P, Kabeláč M, Krumschnabel G, Lukeš M, Voloshko L, Kopecký J & Hrouzek P, The cyanobacterial metabolite nocuolin A is a natural oxadiazine that triggers apoptosis in human cancer cells. *PLoS One,* 12 (2017) e0172850.

32 Sousa ML, Preto M, Vasconcelos V, Linder S & Urbatzka R, Antiproliferative effects of the natural oxadiazine nocuolin A are associated with impairment of mitochondrial oxidative phosphorylation. *Front Oncol,* 9 (2019) 224.

33 Xu XL, Yang YR, Mo XF, Wei JL, Zhang XJ & You QD, Design, synthesis, and evaluation of benzofuran derivatives as novel anti-pancreatic carcinoma agents targeting HIF-1α. *Eur J Med Chem,* 137 (2017) 45.

34 Zhang J, Xu K, Yang F, Qiu Y, Li J, Wang W, Tan G, Zou Z & Kang F, Design, synthesis and evaluation of nitric oxide releasing derivatives of 2, 4-diaminopyrimidine as novel FAK inhibitors for metastatic triple-negative breast cancer. *Eur J Med Chem,* 250 (2023) 115192.

35 Sliwoski G, Kothiwale S, Meiler J & Lowe EW Jr, Computational methods in drug discovery. *Pharmacol Rev,* 66 (2013) 334.

36 Patil R, Das S, Stanley A, Yadav L, Sudhakar A & Varma AK, Optimized hydrophobic interactions and hydrogen bonding at the target–ligand interface lead the pathways of drug designing. *PLoS One,* 5 (2010) e12029.

37 Xu Z, Yang Z, Liu Y, Lu Y, Chen K & Zhu W, Halogen bond: its role beyond drug-target binding affinity for drug discovery and development. *J Chem Inf Model,* 54 (2014) 69.

38 Arnott JA & Planey SL, The influence of lipophilicity in drug discovery and design. *Expert Opin Drug Discov,* 7 (2012) 863.

39 Di L & Kerns EH, *Drug-like Properties: Concepts, Structure Design and Methods from ADME to Toxicity Optimization.* Academic Press, (2015) 1.

40 Savjani KT, Gajjar AK & Savjani JK, Drug solubility: importance and enhancement techniques. *ISRN Pharmaceutics,* 2012 (2012) 195727.

41 Sharom FJ, ABC multidrug transporters: structure, function and role in chemoresistance. *Pharmacogenomics,* 9 (2008) 105.

42 Townsend PD, Rodgers TL, Glover LC, Korhonen HJ, Richards SA, Colwell LJ, Pohl E, Wilson MR, Hodgson DRW, McLeish TCB & Cann MJ, The role of protein–ligand contacts in allosteric regulation of *E. coli* catabolite activator protein. *J Biol Chem,* 290 (2015) 22225.

43 Bryant P, Kelkar A, Guljas A, Clementi C & Noé F, Structure prediction of protein–ligand complexes from sequence information with Umol. *Nat Commun,* 15 (2024) 4536.

44 McNaught AD, *Compendium of Chemical Terminology.* 2nd ed. Oxford: Blackwell Science, (1997) 1.

45 Hao MH, Haq O & Muegge I, Torsion angle preference and energetics of small-molecule ligands bound to proteins. *J Chem Inf Model,* 47(6) (2007) 2242.

46 Goda S, Nafie S, Awad M, Abdel-Kader S, Ibrahim K, Badr M & Eltamany E, *In vitro* and *in vivo* studies of anti-lung cancer activity of *Artemisia judaica* L. crude extract combined with LC-MS/MS profiling, docking simulation and HPLC-DAD quantification. *Antioxidants (Basel),* 11 (2021) 17.

47 Nasr A, Noman M, Mothana A, Alqahtani S & Al-Mishari A, Cytotoxic, antimicrobial and antioxidant activities and phytochemical analysis of *Artemisia judaica* and *A. sieberi* in Saudi Arabia. *Afr J Pharm Pharmacol,* 14 (2020) 278.

48 Fuloria S, Subramaniyan V, Karupiah S, Kumari U, Sathasivam K, Meenakshi DU, Wu YS, Guad RM, Udupa KU & Fuloria NK, A comprehensive review on source, types, effects, nanotechnology, detection, and therapeutic management of reactive carbonyl species. *Antioxidants (Basel),* 9 (2020) 1075.

49 Sarmiento-Salinas FL, Perez-Gonzalez A, Acosta-Casique A, Ix-Ballote A, Diaz A, Treviño S, Rosas-Murrieta NHR, Millán-Perez-Peña L & Maycotte P, Reactive oxygen species: role in carcinogenesis, cancer cell signaling and tumor progression. *Life Sci,* 284 (2021) 119942.

50 Salih AM, Qahtan AA & Al-Qurainy F, Phytochemicals identification and bioactive compounds estimation of *Artemisia* species grown in Saudi Arabia. *Metabolites,* 13 (2023) 443.

51 Benali T, Jaouadi I, Ghchime R, El Omari N, Harboul K, Hammani K, Rebezov M, Shariati MA, Mubarak MS, Simal-Gandara J, Zengin G, Moon-Nyeo P, Kim B, Mahmud S, Learn-Han L & Bouyahya A, The current state of knowledge on biological properties of cirsimaritin. *Antioxidants (Basel),* 11 (2022) 1842.

52 Chen KW, Demarco B, Heilig R, Shkarina K, Boettcher A, Farady CJ & Broz P, Extrinsic and intrinsic apoptosis activate pannexin-1 to drive NLRP3 inflammasome assembly. *EMBO J,* 38 (2019) e101638.

53 Younes M, Bin K, Unissa R, Almarshdi A, Alharbi M, Alenzi S & Abouzied S, *In vitro* evaluation of antimicrobial and cytotoxic activity of *Artemisia judaica* leaves and stem extracts via induction of caspase-dependent apoptosis. *Indian J Pharm Educ Res,* 56 (2022) S52.

54 Kamarya Y, Lijie X & Jinyao L, Chemical constituents and antitumor mechanisms of *Artemisia*. *Anticancer Agents Med Chem,* 22 (2022) 1838.

55 Aboud F, Al-Shaeri M, Zari A, Ali E & Almalki N, Molecular docking and dynamic simulation of phytochemical components from *Clitoria ternatea* against hormone-dependent cancer cell lines. *Indian J Chem,* 64 (2025) 192.